

# Functional effects of schizophrenia-linked genetic variants on intrinsic single-neuron excitability: A modeling study.

Tuomo Mäki-Marttunen<sup>1</sup>, Geir Halnes<sup>2</sup>, Anna Devor<sup>3,4,5</sup>, Aree Witoelar<sup>1</sup>, Francesco Bettella<sup>1,6</sup>, Srdjan Djurovic<sup>7,8</sup>, Yunpeng Wang<sup>1,6</sup>, Gaute T. Einevoll<sup>2,9</sup>, Ole A. Andreassen<sup>1,6</sup>, Anders M. Dale<sup>3,4</sup>

<sup>1</sup>NORMENT, KG Jebsen Centre for Psychosis Research, Institute of Clinical Medicine, University of Oslo, Oslo, Norway

<sup>2</sup>Department of Mathematical Sciences and Technology, Norwegian University of Life Sciences, Ås, Norway

<sup>3</sup>Department of Neurosciences, University of California San Diego, La Jolla, CA, USA

<sup>4</sup>Department of Radiology, University of California, San Diego, La Jolla, CA, USA

<sup>5</sup>Martinos Center for Biomedical Imaging, Massachusetts General Hospital, Harvard Medical School, Charlestown, MA, USA

<sup>6</sup>Division of Mental Health and Addiction, Oslo University Hospital, Oslo, Norway

<sup>7</sup>Department of Medical Genetics, Oslo University Hospital, Oslo, Norway

<sup>8</sup>NORMENT, KG Jebsen Centre for Psychosis Research, Department of Clinical Science, University of Bergen, Bergen, Norway

<sup>9</sup>Department of Physics, University of Oslo, Oslo, Norway

Corresponding author: Anders M. Dale, 8950 VLJ Dr/C-101 La Jolla, CA, USA (amdale@ucsd.edu)

## Abstract

### Background

Recent genome-wide association studies (GWAS) have identified a large number of genetic risk factors for schizophrenia (SCZ) featuring ion channels and calcium transporters. For some of these risk factors, independent prior investigations have examined the effects of genetic alterations on the cellular electrical excitability and calcium homeostasis. In the present proof-of-concept study, we harnessed these experimental results for modeling of computational properties on layer V cortical pyramidal cell and identify possible common alterations in behavior across SCZ-related genes.

### Methods

We applied a biophysically detailed multi-compartmental model to study the excitability of a layer V pyramidal cell. We reviewed the literature on functional genomics for variants of genes associated with SCZ, and used changes in neuron model parameters to represent the effects of these variants.

### Results

We present and apply a framework for examining the effects of subtle single nucleotide polymorphisms in ion channel and Ca<sup>2+</sup> transporter-encoding genes on neuron excitability. Our analysis indicates that most of the considered SCZ-related genetic variants affect the spiking behavior and intracellular calcium dynamics resulting from summation of inputs across the dendritic tree.

### Conclusions

Our results suggest that alteration in the ability of a single neuron to integrate the inputs and scale its excitability may constitute a fundamental mechanistic contributor to mental disease, alongside with the previously proposed deficits in synaptic communication and network behavior.

## Introduction

Schizophrenia (SCZ) is a severe mental disorder with heritability estimates ranging from 0.6 to 0.8 [Ripke et al., 2013]. A recent genome-wide association study (GWAS) has identified more than a hundred genes exceeding genome-wide significance, confirming the polygenic nature of this psychiatric disorder [Ripke et al., 2014]. This remarkable success in gene discovery brings up the next big challenge for psychiatric genetics – translation of the genetic associations into biological insights [van Os and Kapur, 2009]. Attaining this goal is supported by the development of biophysically detailed neuron models, boosted by the recent launch of mega-scale neuroscience projects [Grillner, 2014]. These models make it possible to investigate SCZ disease mechanisms by computational means, ultimately aiming towards achieving better clinical treatments and disorder outcomes [Wang and Krystal, 2014, Owen, 2014].

The 108 recently confirmed SCZ-linked loci span a wide set of protein-coding genes [Ripke et al., 2014], including numerous ion channel-encoding genes. The disorder is associated with genes affecting transmembrane currents of all

major ionic species,  $\text{Na}^+$ ,  $\text{K}^+$ , and  $\text{Ca}^{2+}$ . In addition, some of the SCZ-linked genes are involved in regulation of the  $\text{Ca}^{2+}$  concentration in the intracellular medium [Ripke et al., 2014], which is another great contributor to excitability. It is thus reasonable to hypothesize that the SCZ-linked genes should have an impact on the excitability at the single neuron level.

We focus our study on cortical layer V pyramidal cells (L5PC) as a principal computational element of the cerebral circuit. An L5PC extends throughout the cortical depth with the soma located in layer V and the apical dendrite branching into the “apical tuft” in layer I, and its long axon may project to non-local cortical and subcortical areas. The tuft serves as an integration hub for long-distance synaptic inputs, and is often considered a biological substrate for cortical associations providing high-level “context” for low-level (e.g., sensory) inputs to the perisomatic compartment [Larkum, 2013]. Therefore, the ability of L5PC to communicate the apical inputs to the soma has been proposed as one of the mechanisms that could be impaired in the mental disease [Larkum, 2013]. In agreement with this hypothesis, recent psychiatric GWASs consistently reported association of genes coding for the subunits of voltage-gated  $\text{Ca}^{2+}$  channels as risk factors in SCZ and bipolar disorder [Sklar et al., 2011, Ripke et al., 2011, Smoller et al., 2013].

In the present proof-of-principle study, we apply a model [Hay et al., 2011] of L5PC to explore how genetic variants in SCZ-linked genes affect the single-cell excitability. We carry out our study by linking a documented effect of a genetic variant in an ion channel or  $\text{Ca}^{2+}$  transporter-encoding gene to a change in the corresponding neuron model parameter. It should, however, be noted that information does not generally exist for the effect of single nucleotide polymorphism (SNP) variants identified through GWASs on the biophysical parameters required for the computational models. We instead use information obtained from *in vitro* studies of more extreme genetic variations, including loss of function mutations. A central assumption of this approach is that the effects of SNP variants can be represented as scaled-down versions of those of the more extreme variants, and that the emergence of the full psychiatric disease phenotype results from the combined effect of a large number of subtle SNP effects [Gottesman and Shields, 1967, Purcell et al., 2009]. A deficit in synaptic communication is likely to contribute to SCZ [Stefansson et al., 2009, Fromer et al., 2014, Wen et al., 2014, Ripke et al., 2014] but is outside the scope of the present work.

## Methods and materials

### The L5PC model

The multi-compartmental neuron model used in this work is based on a reconstructed morphology of a layer V thick-tufted pyramidal neuron (cell #1 in [Hay et al., 2011]). The model includes the following ionic currents: Fast inactivating  $\text{Na}^+$  current ( $I_{\text{Nat}}$ ), persistent  $\text{Na}^+$  current ( $I_{\text{Nap}}$ ), non-specific cation current ( $I_h$ ), muscarinic  $\text{K}^+$  current ( $I_m$ ), slow inactivating  $\text{K}^+$  current ( $I_{\text{Kp}}$ ), fast inactivating  $\text{K}^+$  current ( $I_{\text{Kt}}$ ), fast non-inactivating  $\text{K}^+$  current ( $I_{\text{Kv3.1}}$ ), high-voltage-activated  $\text{Ca}^{2+}$  current ( $I_{\text{CaHVA}}$ ), low-voltage-activated  $\text{Ca}^{2+}$  current ( $I_{\text{CaLVA}}$ ), small-conductance  $\text{Ca}^{2+}$ -activated  $\text{K}^+$  current ( $I_{\text{SK}}$ ), and finally, the passive leak current ( $I_{\text{leak}}$ ). See Supplemental information for the model equations, and for the simulation codes, see ModelDB entry 169457 (<https://senselab.med.yale.edu/ModelDB>).

### Genes included in the study

Since we did not aim to provide a comprehensive evaluation of a representative fraction of the genetic risk factors of SCZ, but to provide a proof of principle of the computational modeling approach, we selected the genomic loci using the following approach. We based our study on the recent GWAS [Ripke et al., 2014], which reported significantly associated SNPs that were scattered across hundreds of genes with a variety of cellular functions. We concentrated on those genes that encoded either ionic channels or proteins contributing to transportation of intracellular  $\text{Ca}^{2+}$  ions.

We used the SNP-wise p-value data of [Ripke et al., 2014], and for each gene of interest, determined the minimum p-value among those SNPs that were located in the considered gene. We performed this operation for all genes encoding either subunits of voltage-gated  $\text{Ca}^{2+}$ ,  $\text{K}^+$ , or  $\text{Na}^+$  channel, subunits of an SK, leak, or hyperpolarization-activated cyclic nucleotide-gated (HCN) channel, or  $\text{Ca}^{2+}$ -transporting ATPases. The genes *CACNA1C*, *CACNB2*, *CACNA1I*, *ATP2A2*, and *HCN1* possessed a small minimum p-value each ( $p < 3 \times 10^{-8}$ ) — these genes were also highlighted in the locus-oriented association analysis as performed in [Ripke et al., 2014]. In order to extend our study to explore a larger set of genes, we used a more relaxed threshold ( $p < 3 \times 10^{-5}$ ) for the minimum p-value, and obtained the following genes in addition to the previously mentioned ones: *CACNA1D*, *CACNA1S*, *SCN1A*, *SCN7A*, *SCN9A*, *KCNN3*, *KCNS3*, *KCNB1*, *KCNG2*, *KCNH7*, and *ATP2B2*. Of these, we omitted the genes that are not relevant for the firing behavior of an L5PC. It should be noted that we used the SNPs reported in [Ripke et al., 2014] only to name the above SCZ-related genes, and due to lack of functional genomics data, we could not include the actual SCZ-related SNPs in our simulation study. Instead, we searched in PubMed for functional genomic studies reporting the effects of any genetic variant of the above genes. For details, see Supplemental information.

## Results

### A new framework for bridging the gap between GWASs of SCZ and computational neuroscience

In this work, we reviewed the literature on effects of variants in SCZ-related genes on ion channel behavior and intracellular  $\text{Ca}^{2+}$  dynamics, and interpreted the reported effects in the context of our neuron model parameters. An overview of the relevant studies is given in Table 1, while the effects of each variant on the L5PC model parameters are given in Table 2. These data gave us a direct interface for linking a change in the genomic data, such as a SNP or an alternative splicing, into a change in neuron dynamics. The reported data, however, often corresponded to variants with large phenotypic consequences that in general are absent in SCZ patients. To simulate subtle cellular effects caused by the common SNPs related to SCZ [Lee et al., 2012], we downscaled the variants of Table 2 by bringing the changed parameters closer to the control neuron values when the reported change caused too large an effect in the neuron firing behavior. Our approach is illustrated in Figure 1.

Table 1: **Table of the genetic variants used in this study.** For more details, see Table 2.

Gene	Refs.	Type of variant	Cell type
<i>CACNA1C</i>	[Kudrnc et al., 2009]	L429T, L434T, S435T, S435A, S435P	TSA201
<i>CACNA1C</i>	[Kudrnc et al., 2009]	L779T, I781T, I781P	TSA201
<i>CACNB2</i>	[Cordeiro et al., 2009]	T11I-mutant	TSA201
<i>CACNB2</i>	[Massa et al., 1995]	A1B2 vs A1 alone	HEK293
<i>CACNB2</i>	[Link et al., 2009]	N1 vs N3 vs N4 vs N5	HEK293
<i>CACNA1D</i>	[Tan et al., 2011], [Bock et al., 2011]	42A splices transfected	TSA201/HEK293
<i>CACNA1D</i>	[Tan et al., 2011], [Bock et al., 2011]	43S splices transfected	TSA201/HEK293
<i>CACNA1D</i>	[Zhang et al., 2011], [Pérez-Alvarez et al., 2011]	Homozyg. knockout	AV node cells / chromaffin cells
<i>CACNA1I</i>	[Murbartián et al., 2004]	Alternative splicing of exons 9 and 33	HEK293
<i>ATP2A2</i>	[Ji et al., 2000]	Heter. null mutation	myocytes
<i>ATP2B2</i>	[Fakira et al., 2012]	Heter. knockout	Purkinje cells
<i>ATP2B2</i>	[Empson et al., 2010]	Homozyg. knockout	Purkinje cells
<i>ATP2B2</i>	[Ficarella et al., 2007]	G283S-,G293S-mutant	CHO cells
<i>SCN1A</i>	[Cestèle et al., 2008]	FHM mutation Q1489K	Cultured neocortical cell
<i>SCN1A</i>	[Vanmolkot et al., 2007]	FHM mutation L1649Q	TSA201
<i>SCN9A</i>	[Estacion et al., 2011]	I228M NaV1.7 variant	HEK293
<i>SCN9A</i>	[Estacion et al., 2008]	A1632E NaV1.7 mutation	HEK293
<i>SCN9A</i>	[Han et al., 2006]	L858F NaV1.7 mutation	HEK293
<i>SCN9A</i>	[Dib-Hajj et al., 2005]	F1449V NaV1.7 mutation	HEK293
<i>KCNS3</i>	[Shepard and Rae, 1999]	hKv2.1-(G4S)3-hKv9 fusion inserted	HEK293
<i>KCNB1</i>	[Bocksteins et al., 2011]	T203K, T203D, S347K, S347D, T203W, S347W	LTK-
<i>KCNN3</i>	[Wittekindt et al., 2004]	hSK3.ex4 isoform	TSA
<i>HCN1</i>	[Ishii et al., 2007]	D135W, D135H, D135N mutants	HEK293

The variants in Table 1 were 23 in total, although some of them represented a range of effects of different variants (see Supplemental information, Table S1). The entries corresponded to variants of genes encoding for  $\text{Ca}^{2+}$  channel subunits (*CACNA1C*, *CACNB2*, *CACNA1D*, *CACNA1I*), intracellular  $\text{Ca}^{2+}$  pumps (*ATP2A2*, *ATP2B2*),  $\text{Na}^+$  channel subunits (*SCN1A*, *SCN9A*),  $\text{K}^+$  channel subunits (*KCNS3*, *KCNB1*, *KCNN3*), and a non-specific ion channel subunit (*HCN1*). In the following, we present simulation results for the L5PC model equipped with some of these downscaled variants (we refer to these model neurons as “variant neurons” or simply as “variants”). As we do not know the quality of the effects of the actual SCZ-related polymorphisms, we perform the simulations for a range of differently scaled variants, including negative scalings (i.e. opposite effects w.r.t. the effects reported in Table 2). We concentrated our study on a representative sample of six variants, highlighted in Table 2. These variants represent six genes with different roles in L5PC electrogenesis and a wide range of observed effects (see Table S2).

### Variants show altered intracellular $[\text{Ca}^{2+}]$ responses to short stimuli

To characterize the implications of SCZ-related genes on the neuron excitability, we started by analyzing the effects of the downscaled versions of genetic variants in Table 2 on the neuron response to a short somatic suprathreshold square-pulse stimulus. Figure 2A-B shows the time course of the membrane potential and the intracellular  $\text{Ca}^{2+}$ -concentration ( $[\text{Ca}^{2+}]$ ) for one variant, whereas Figure 2C shows the  $[\text{Ca}^{2+}]$  response in the phase plane for several different variants. The most typical effect of a variant was a deviation in the peak  $[\text{Ca}^{2+}]$ , but differences could also be observed in the rising phase of the  $[\text{Ca}^{2+}]$ , as shown in the phase plane representation in Figure 2C.

The results in Figure 2 show that the  $[\text{Ca}^{2+}]$  response served as a more sensitive indicator of genetic effects than the membrane potential. In *CACNA1C* and *CACNB2* variants, which affect the high-voltage-activated (HVA)  $\text{Ca}^{2+}$

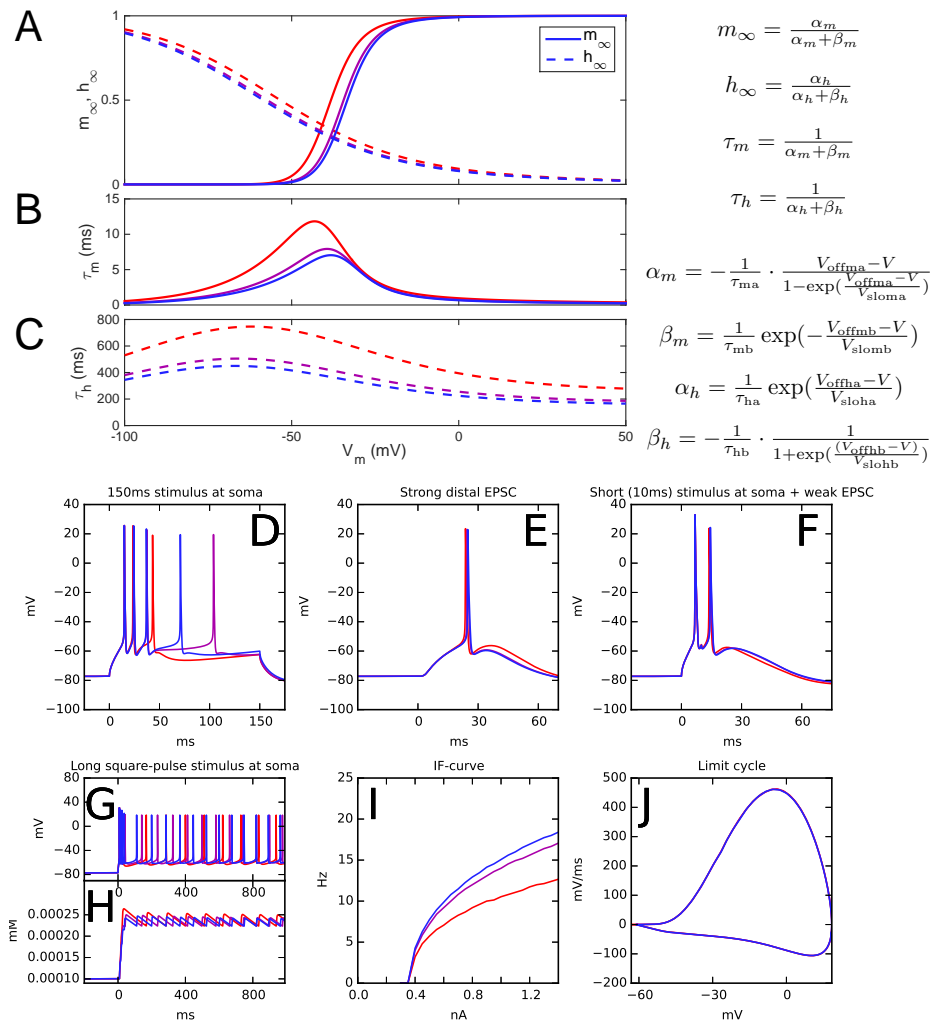


Figure 1: **An example of downscaling with a variant [Link et al., 2009] of the gene *CACNB2*.** The authors of [Link et al., 2009] transfected different variants of *CACNB2* DNA into HEK293 cells together with CaV1.2 subunit DNA, and measured the activation and inactivation curves of the Ca<sup>2+</sup> currents through the cell membrane. The cells transfected with different variants showed different values of mid-points and time constants for channel activation and inactivation: The mid-points of activation and inactivation varied by  $\pm 4.9$  and  $\pm 5.1$  mV among the variants, respectively, while the time constants of activation and inactivation varied from  $-40\%$  to  $+68\%$  and  $-40\%$  to  $+66\%$ , respectively. Here we illustrate a variant representing one possible combination of the endpoints of these ranges. **A:** The voltage-dependence of steady-state activation ( $m_\infty$ ) and inactivation ( $h_\infty$ ) according to the neuron model [Hay et al., 2011]. Red curves represent the unscaled variant: Activation parameters  $V_{offma}$  and  $V_{offmb}$  are changed by  $\Delta_1 = -4.9$  mV, inactivation parameters  $V_{offha}$  and  $V_{offhb}$  are changed by  $\Delta_2 = 5.1$  mV, activation time constants  $\tau_{ma}$  and  $\tau_{mb}$  are increased by 68% ( $\eta_3 = 1.68$ ), and inactivation time constants  $\tau_{ha}$  and  $\tau_{hb}$  are increased by +66% ( $\eta_4 = 1.66$ ). Purple curves show the downscaled  $\epsilon = \frac{1}{2}$  variant (see below), and blue curves show the control neuron activation properties. **B–C:** The voltage-dependence of time constants for activation (B) and inactivation (C). **D–J:** Illustration of the scaling conditions. The downscaling is based on five conditions (see Supplemental information), none of which should be violated in the downscaled variant. In panels (D)–(F) (conditions I–III), the variant neuron should respond with the same number of spikes as the control neuron (blue). In panel (I), the integrated difference between the variant and control f-I curves should not exceed 10% of the integral of the control curve (condition IV). In panel (J), the difference between the limit cycles should not exceed a set limit (condition V). It can be observed that the unscaled variant (red) violates the conditions I and IV. To scale down the variant, each applied parameter change is brought to a fraction  $c < 1$ , all in proportion, until the threshold of violating/non-violating variant is found. In this example, the threshold variant corresponds to parameter changes  $c \times \Delta_1$ ,  $c \times \Delta_2$ ,  $\eta_3^c$ , and  $\eta_4^c$ , where  $c = 0.4574$ . Any non-negative value below the threshold value  $c$  yields a downscaled variant that obeys conditions I–V. The purple curves represent the variant corresponding to parameter changes  $c\epsilon \times \Delta_1$ ,  $c\epsilon \times \Delta_2$ ,  $\eta_3^{c\epsilon}$ , and  $\eta_4^{c\epsilon}$ , where  $c = 0.4574$  and  $\epsilon = \frac{1}{2}$ . The blue curves show the control neuron firing behavior. (D): Somatic membrane potential as a response to a 150ms somatic square-pulse stimulus (0.696 nA). (E): Somatic response to a distal apical synaptic conductance with maximum 0.0612  $\mu$ S. (F): Somatic response to a combination of somatic square-pulse current (10 ms  $\times$  1.137 nA) and a distal apical synaptic conductance (maximum 0.100  $\mu$ S). (G): Somatic membrane potential as a response to a long somatic square-pulse stimulus current (1.0 nA). (H): Somatic Ca<sup>2+</sup> concentration as a response to the stimulus used in (G). (I): Spiking frequency as a function of amplitude of the somatic DC. (J): The membrane potential limit cycle corresponding to the late phase of (G). The x-axis represents the somatic membrane potential and y-axis its time derivative.

Table 2: **List of variants and their threshold effect coefficients  $c$ .** The variants are ordered as in Table 1, but the variants where several combinations of parameter range end points were considered are listed as separate variants (see Supplemental information). The variants marked with † were used in Figures 2–6, the variants marked with § were used in Figure S3, and the variant marked with ‡ was used in Figure 1.

Gene	Effect on model parameters	Thresh. effect
<i>CACNA1C</i>	$V_{\text{offm}*,\text{CaHVA}}: -25.9 \text{ mV}; V_{\text{offh}*,\text{CaHVA}}: -27.0 \text{ mV}$	$c = 0.094$
<i>CACNA1C</i>	$V_{\text{offm}*,\text{CaHVA}}: -37.3 \text{ mV}; V_{\text{offh}*,\text{CaHVA}}: -30.0 \text{ mV}$	$c = 0.060$ †
<i>CACNB2</i>	$V_{\text{offh}*,\text{CaHVA}}: -5.2 \text{ mV}; V_{\text{sloh}*,\text{CaHVA}}: \times 0.69$	$c = 0.582$
<i>CACNB2</i>	$\tau_{\text{h}*,\text{CaHVA}}: \times 1.7$	$c \geq 2.000$
<i>CACNB2</i>	$V_{\text{offm}*,\text{CaHVA}}: -4.9 \text{ mV}; V_{\text{offh}*,\text{CaHVA}}: -5.1 \text{ mV}; \tau_{\text{m}*,\text{CaHVA}}: \times 0.6; \tau_{\text{h}*,\text{CaHVA}}: \times 0.6$	$c = 0.310$
	$V_{\text{offm}*,\text{CaHVA}}: +4.9 \text{ mV}; V_{\text{offh}*,\text{CaHVA}}: -5.1 \text{ mV}; \tau_{\text{m}*,\text{CaHVA}}: \times 0.6; \tau_{\text{h}*,\text{CaHVA}}: \times 0.6$	$c = 0.154$
	$V_{\text{offm}*,\text{CaHVA}}: -4.9 \text{ mV}; V_{\text{offh}*,\text{CaHVA}}: +5.1 \text{ mV}; \tau_{\text{m}*,\text{CaHVA}}: \times 0.6; \tau_{\text{h}*,\text{CaHVA}}: \times 0.6$	$c = 0.205$
	$V_{\text{offm}*,\text{CaHVA}}: +4.9 \text{ mV}; V_{\text{offh}*,\text{CaHVA}}: +5.1 \text{ mV}; \tau_{\text{m}*,\text{CaHVA}}: \times 0.6; \tau_{\text{h}*,\text{CaHVA}}: \times 0.6$	$c = 0.675$ §
	$V_{\text{offm}*,\text{CaHVA}}: -4.9 \text{ mV}; V_{\text{offh}*,\text{CaHVA}}: -5.1 \text{ mV}; \tau_{\text{m}*,\text{CaHVA}}: \times 1.68; \tau_{\text{h}*,\text{CaHVA}}: \times 0.6$	$c = 0.814$
	$V_{\text{offm}*,\text{CaHVA}}: +4.9 \text{ mV}; V_{\text{offh}*,\text{CaHVA}}: -5.1 \text{ mV}; \tau_{\text{m}*,\text{CaHVA}}: \times 1.68; \tau_{\text{h}*,\text{CaHVA}}: \times 0.6$	$c = 0.057$
	$V_{\text{offm}*,\text{CaHVA}}: -4.9 \text{ mV}; V_{\text{offh}*,\text{CaHVA}}: +5.1 \text{ mV}; \tau_{\text{m}*,\text{CaHVA}}: \times 1.68; \tau_{\text{h}*,\text{CaHVA}}: \times 0.6$	$c = 0.517$
	$V_{\text{offm}*,\text{CaHVA}}: +4.9 \text{ mV}; V_{\text{offh}*,\text{CaHVA}}: +5.1 \text{ mV}; \tau_{\text{m}*,\text{CaHVA}}: \times 1.68; \tau_{\text{h}*,\text{CaHVA}}: \times 0.6$	$c = 0.078$
	$V_{\text{offm}*,\text{CaHVA}}: -4.9 \text{ mV}; V_{\text{offh}*,\text{CaHVA}}: -5.1 \text{ mV}; \tau_{\text{m}*,\text{CaHVA}}: \times 0.6; \tau_{\text{h}*,\text{CaHVA}}: \times 1.66$	$c = 0.275$
	$V_{\text{offm}*,\text{CaHVA}}: +4.9 \text{ mV}; V_{\text{offh}*,\text{CaHVA}}: -5.1 \text{ mV}; \tau_{\text{m}*,\text{CaHVA}}: \times 0.6; \tau_{\text{h}*,\text{CaHVA}}: \times 1.66$	$c = 0.188$
	$V_{\text{offm}*,\text{CaHVA}}: -4.9 \text{ mV}; V_{\text{offh}*,\text{CaHVA}}: +5.1 \text{ mV}; \tau_{\text{m}*,\text{CaHVA}}: \times 0.6; \tau_{\text{h}*,\text{CaHVA}}: \times 1.66$	$c = 0.190$
	$V_{\text{offm}*,\text{CaHVA}}: +4.9 \text{ mV}; V_{\text{offh}*,\text{CaHVA}}: +5.1 \text{ mV}; \tau_{\text{m}*,\text{CaHVA}}: \times 0.6; \tau_{\text{h}*,\text{CaHVA}}: \times 1.66$	$c = 1.687$
	$V_{\text{offm}*,\text{CaHVA}}: -4.9 \text{ mV}; V_{\text{offh}*,\text{CaHVA}}: -5.1 \text{ mV}; \tau_{\text{m}*,\text{CaHVA}}: \times 1.68; \tau_{\text{h}*,\text{CaHVA}}: \times 1.66$	$c = 0.707$
	$V_{\text{offm}*,\text{CaHVA}}: +4.9 \text{ mV}; V_{\text{offh}*,\text{CaHVA}}: -5.1 \text{ mV}; \tau_{\text{m}*,\text{CaHVA}}: \times 1.68; \tau_{\text{h}*,\text{CaHVA}}: \times 1.66$	$c = 0.061$
	$V_{\text{offm}*,\text{CaHVA}}: -4.9 \text{ mV}; V_{\text{offh}*,\text{CaHVA}}: +5.1 \text{ mV}; \tau_{\text{m}*,\text{CaHVA}}: \times 1.68; \tau_{\text{h}*,\text{CaHVA}}: \times 1.66$	$c = 0.457$ † ‡
	$V_{\text{offm}*,\text{CaHVA}}: +4.9 \text{ mV}; V_{\text{offh}*,\text{CaHVA}}: +5.1 \text{ mV}; \tau_{\text{m}*,\text{CaHVA}}: \times 1.68; \tau_{\text{h}*,\text{CaHVA}}: \times 1.66$	$c = 0.084$
<i>CACNA1D</i>	$V_{\text{offm}*,\text{CaHVA}}: -10.9 \text{ mV}; V_{\text{slo}*,\text{CaHVA}}: \times 0.73; V_{\text{offh}*,\text{CaHVA}}: -3.0 \text{ mV}; V_{\text{sloh}*,\text{CaHVA}}: \times 0.81; \tau_{\text{h}*,\text{CaHVA}}: \times 1.25$	$c = 0.118$
	$V_{\text{offm}*,\text{CaHVA}}: -10.9 \text{ mV}; V_{\text{slo}*,\text{CaHVA}}: \times 0.73; V_{\text{offh}*,\text{CaHVA}}: +3.5 \text{ mV}; V_{\text{sloh}*,\text{CaHVA}}: \times 0.81; \tau_{\text{h}*,\text{CaHVA}}: \times 1.25$	$c = 0.106$
<i>CACNA1D</i>	$V_{\text{offm}*,\text{CaHVA}}: -10.6 \text{ mV}; V_{\text{slo}*,\text{CaHVA}}: \times 0.8; V_{\text{offh}*,\text{CaHVA}}: -5.3 \text{ mV}; V_{\text{sloh}*,\text{CaHVA}}: \times 0.66; \tau_{\text{h}*,\text{CaHVA}}: \times 0.72$	$c = 0.114$
	$V_{\text{offm}*,\text{CaHVA}}: +3.4 \text{ mV}; V_{\text{slo}*,\text{CaHVA}}: \times 0.8; V_{\text{offh}*,\text{CaHVA}}: -5.3 \text{ mV}; V_{\text{sloh}*,\text{CaHVA}}: \times 0.66; \tau_{\text{h}*,\text{CaHVA}}: \times 0.72$	$c = 1.962$
	$V_{\text{offm}*,\text{CaHVA}}: -10.6 \text{ mV}; V_{\text{slo}*,\text{CaHVA}}: \times 1.12; V_{\text{offh}*,\text{CaHVA}}: -5.3 \text{ mV}; V_{\text{sloh}*,\text{CaHVA}}: \times 0.66; \tau_{\text{h}*,\text{CaHVA}}: \times 0.72$	$c = 0.131$
	$V_{\text{offm}*,\text{CaHVA}}: +3.4 \text{ mV}; V_{\text{slo}*,\text{CaHVA}}: \times 1.12; V_{\text{offh}*,\text{CaHVA}}: -5.3 \text{ mV}; V_{\text{sloh}*,\text{CaHVA}}: \times 0.66; \tau_{\text{h}*,\text{CaHVA}}: \times 0.72$	$c = 0.601$
	$V_{\text{offm}*,\text{CaHVA}}: -10.6 \text{ mV}; V_{\text{slo}*,\text{CaHVA}}: \times 0.8; V_{\text{offh}*,\text{CaHVA}}: +1.2 \text{ mV}; V_{\text{sloh}*,\text{CaHVA}}: \times 0.66; \tau_{\text{h}*,\text{CaHVA}}: \times 0.72$	$c = 0.100$
	$V_{\text{offm}*,\text{CaHVA}}: +3.4 \text{ mV}; V_{\text{slo}*,\text{CaHVA}}: \times 0.8; V_{\text{offh}*,\text{CaHVA}}: +1.2 \text{ mV}; V_{\text{sloh}*,\text{CaHVA}}: \times 0.66; \tau_{\text{h}*,\text{CaHVA}}: \times 0.72$	$c = 0.645$
	$V_{\text{offm}*,\text{CaHVA}}: -10.6 \text{ mV}; V_{\text{slo}*,\text{CaHVA}}: \times 1.12; V_{\text{offh}*,\text{CaHVA}}: +1.2 \text{ mV}; V_{\text{sloh}*,\text{CaHVA}}: \times 0.66; \tau_{\text{h}*,\text{CaHVA}}: \times 0.72$	$c = 0.116$
	$V_{\text{offm}*,\text{CaHVA}}: +3.4 \text{ mV}; V_{\text{slo}*,\text{CaHVA}}: \times 1.12; V_{\text{offh}*,\text{CaHVA}}: +1.2 \text{ mV}; V_{\text{sloh}*,\text{CaHVA}}: \times 0.66; \tau_{\text{h}*,\text{CaHVA}}: \times 0.72$	$c = 1.117$
<i>CACNA1D</i>	$V_{\text{offm}*,\text{CaHVA}}: +6.6 \text{ mV}; V_{\text{slo}*,\text{CaHVA}}: \times 0.75; \tau_{\text{h}*,\text{CaHVA}}: \times 0.5$	$c = 0.104$
	$V_{\text{offm}*,\text{CaHVA}}: +6.6 \text{ mV}; V_{\text{slo}*,\text{CaHVA}}: \times 1.19; \tau_{\text{h}*,\text{CaHVA}}: \times 0.5$	$c = 0.068$
	$V_{\text{offm}*,\text{CaHVA}}: +6.6 \text{ mV}; V_{\text{slo}*,\text{CaHVA}}: \times 0.75; \tau_{\text{h}*,\text{CaHVA}}: \times 1.12$	$c = 0.115$ §
	$V_{\text{offm}*,\text{CaHVA}}: +6.6 \text{ mV}; V_{\text{slo}*,\text{CaHVA}}: \times 1.19; \tau_{\text{h}*,\text{CaHVA}}: \times 1.12$	$c = 0.072$
<i>CACNA1I</i>	$V_{\text{offma},\text{CaLVA}}: +1.3 \text{ mV}; V_{\text{offha},\text{CaLVA}}: +1.6 \text{ mV}; \tau_{\text{m}*,\text{CaLVA}}: \times 0.87; \tau_{\text{h}*,\text{CaLVA}}: \times 0.8$	$c \geq 2.000$
	$V_{\text{offma},\text{CaLVA}}: +1.3 \text{ mV}; V_{\text{offha},\text{CaLVA}}: +1.6 \text{ mV}; \tau_{\text{m}*,\text{CaLVA}}: \times 1.45; \tau_{\text{h}*,\text{CaLVA}}: \times 0.8$	$c \geq 2.000$ † §
<i>ATP2A2</i>	$\gamma_{\text{CaDynamics}}: \times 0.6$	$c = 0.093$ §
<i>ATP2B2</i>	$\tau_{\text{decay},\text{CaDynamics}}: \times 1.97$	$c = 0.218$
<i>ATP2B2</i>	$\tau_{\text{decay},\text{CaDynamics}}: \times 1.5; c_{\text{min},\text{CaDynamics}}: \times 1.4$	$c = 0.215$ †
<i>ATP2B2</i>	$\tau_{\text{decay},\text{CaDynamics}}: \times 4.45$	$c = 0.099$
<i>SCN1A</i>	$V_{\text{offm},\text{Nat}}: -0.3 \text{ mV}; V_{\text{offh},\text{Nat}}: +5 \text{ mV}; V_{\text{slo}*,\text{Nat}}: \times 1.15; V_{\text{sloh},\text{Nat}}: \times 1.23$	$c = 0.056$ †
<i>SCN1A</i>	$V_{\text{offm},\text{Nat}}: +2.8 \text{ mV}; V_{\text{offh},\text{Nat}}: +9.6 \text{ mV}; V_{\text{slo}*,\text{Nat}}: \times 0.984; V_{\text{sloh},\text{Nat}}: \times 1.042$	$c = 0.069$
<i>SCN9A</i>	$V_{\text{offh},\text{Nap}}: +6.8 \text{ mV}$	$c \geq 2.000$
<i>SCN9A</i>	$V_{\text{offh},\text{Nap}}: +3.5 \text{ mV}; V_{\text{sloh},\text{Nap}}: \times 0.55; V_{\text{offm},\text{Nat}}: -7.1 \text{ mV}; V_{\text{offh},\text{Nat}}: +17.0 \text{ mV}; V_{\text{sloh},\text{Nat}}: \times 0.69$	$c = 0.026$
<i>SCN9A</i>	$V_{\text{offm},\text{Nat}}: -9.1 \text{ mV}; V_{\text{offh},\text{Nat}}: +3.1 \text{ mV}$	$c = 0.043$
<i>SCN9A</i>	$V_{\text{offm},\text{Nat}}: -7.6 \text{ mV}; V_{\text{offh},\text{Nat}}: +4.3 \text{ mV}$	$c = 0.043$
<i>KCNS3</i>	$\tau_{\text{m}*,\text{Kp}}: \times 2.0; \tau_{\text{h}*,\text{Kp}}: \times 2.5; V_{\text{sloh},\text{Kp}}: \times 0.5$	$c \geq 2.000$
<i>KCNB1</i>	$V_{\text{offm},\text{Kp}}: +5 \text{ mV}; V_{\text{offh},\text{Kp}}: +3 \text{ mV}; V_{\text{slo}*,\text{Kp}}: \times 1.11; V_{\text{sloh},\text{Kp}}: \times 0.86; \tau_{\text{m}*,\text{Kp}}: \times 0.5; \tau_{\text{h}*,\text{Kp}}: \times 0.53$	$c \geq 2.000$
<i>KCNB1</i>	$V_{\text{offm},\text{Kp}}: +1 \text{ mV}; V_{\text{offh},\text{Kp}}: -6 \text{ mV}; V_{\text{slo}*,\text{Kp}}: \times 1.22; V_{\text{sloh},\text{Kp}}: \times 1.0; \tau_{\text{m}*,\text{Kp}}: \times 0.89; \tau_{\text{h}*,\text{Kp}}: \times 1.13$	$c \geq 2.000$
<i>KCNB1</i>	$V_{\text{offm},\text{Kp}}: +6 \text{ mV}; V_{\text{offh},\text{Kp}}: -8 \text{ mV}; V_{\text{slo}*,\text{Kp}}: \times 1.33; V_{\text{sloh},\text{Kp}}: \times 1.0; \tau_{\text{m}*,\text{Kp}}: \times 0.5; \tau_{\text{h}*,\text{Kp}}: \times 0.87$	$c \geq 2.000$
<i>KCNB1</i>	$V_{\text{offm},\text{Kp}}: -28 \text{ mV}; V_{\text{offh},\text{Kp}}: -27 \text{ mV}; V_{\text{slo}*,\text{Kp}}: \times 1.11; V_{\text{sloh},\text{Kp}}: \times 0.71; \tau_{\text{m}*,\text{Kp}}: \times 1.13; \tau_{\text{h}*,\text{Kp}}: \times 2.27$	$c \geq 2.000$
<i>KCNB1</i>	$V_{\text{offm},\text{Kp}}: +14 \text{ mV}; V_{\text{offh},\text{Kp}}: -21 \text{ mV}; V_{\text{slo}*,\text{Kp}}: \times 2.0; V_{\text{sloh},\text{Kp}}: \times 1.0; \tau_{\text{m}*,\text{Kp}}: \times 0.39; \tau_{\text{h}*,\text{Kp}}: \times 1.2$	$c \geq 2.000$
<i>KCNB1</i>	$V_{\text{offm},\text{Kp}}: -13 \text{ mV}; V_{\text{offh},\text{Kp}}: -13 \text{ mV}; V_{\text{slo}*,\text{Kp}}: \times 1.33; V_{\text{sloh},\text{Kp}}: \times 0.71; \tau_{\text{m}*,\text{Kp}}: \times 0.95; \tau_{\text{h}*,\text{Kp}}: \times 5.13$	$c \geq 2.000$
<i>KCNN3</i>	$c_{\text{off},\text{SK}}: \times 0.86; c_{\text{slo},\text{SK}}: \times 1.24$	$c = 1.715$ † §
<i>HCN1</i>	$V_{\text{offma},\text{Ih}}, V_{\text{offmb},\text{Ih}}: -26.5 \text{ mV}; V_{\text{slo}*,\text{Ih}}, V_{\text{sloh},\text{Ih}}: \times 0.64$	$c = 0.296$

current, and in *CACNA1I* variant affecting the low-voltage-activated (LVA)  $\text{Ca}^{2+}$  current, the observed effects on the  $[\text{Ca}^{2+}]$  response were due to changed  $\text{Ca}^{2+}$  channel kinetics. Similarly, in the *ATP2B2* variant, which affects the plasma membrane  $\text{Ca}^{2+}$  ATPase (PMCA) activity, the observed effect was caused by altered intracellular  $\text{Ca}^{2+}$  dynamics. By contrast, the small yet observable differences between control and *SCN1A* variant  $[\text{Ca}^{2+}]$  phase planes were due to alterations in subthreshold membrane potential fluctuations, which caused variation in the activation of  $\text{Ca}^{2+}$  channels.

## Steady-state firing is influenced by the variants

Next, we investigated the steady-state behavior of the neuron when a direct current (DC) was applied to the soma. As shown in Figure 3, the f-I curves (firing frequency as a function of DC amplitude) of many SCZ-associated variants were notably different from those obtained with the control neuron.

The deviations in the f-I curves in many of the variants can be explained by changes in the  $\text{Ca}^{2+}$ -activated SK current. These changes were caused either by direct alteration of the activation kinetics of SK channels (as in the *KCNN3* variant), or indirectly, through the changes in the intracellular  $[\text{Ca}^{2+}]$  response associated with other variants (*CACNA1C*, *CACNB2* and *ATP2B2*). As an example, the  $\text{Ca}^{2+}$  influx during an action potential was larger in the *CACNA1C* variant neuron compared to the control neuron (compare curves in blue and magenta in Figure 2C), and

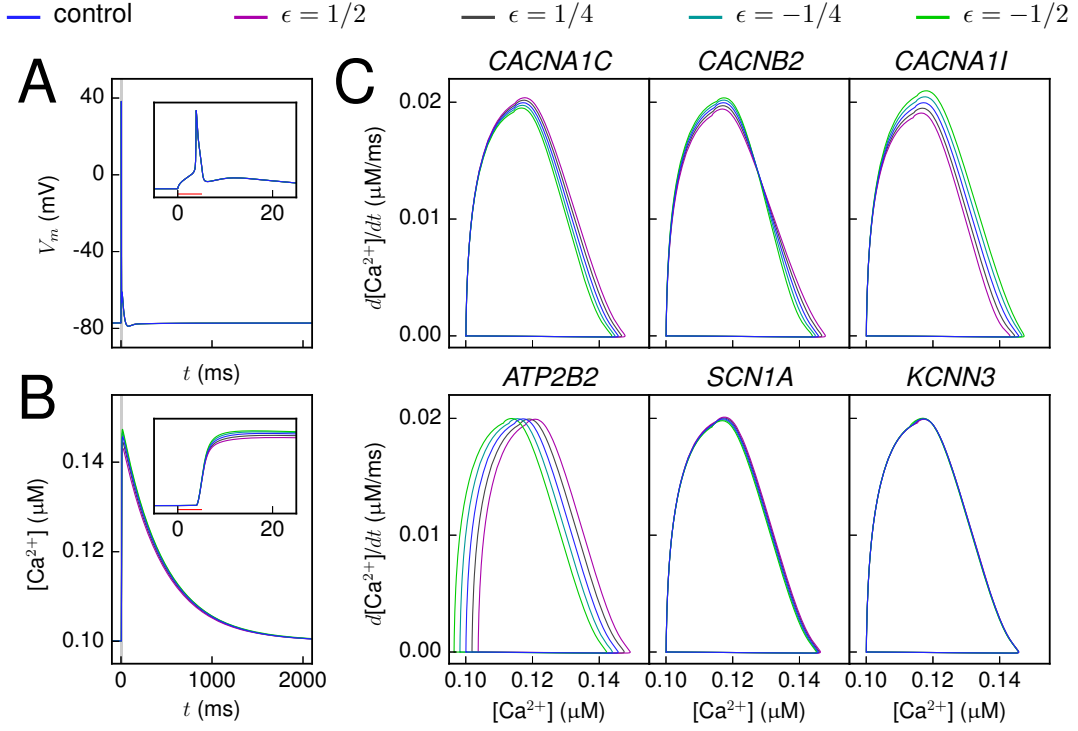


Figure 2: **Variants show altered  $[Ca^{2+}]$  response to a short, somatic stimulus.** **A,B:** The membrane potential (A) and  $Ca^{2+}$  concentration (B) time courses, recorded at soma, as a response to a somatic 5 ms, 1.626 nA square-pulse stimulus. The blue curve shows the control neuron behavior, while the other curves show the behavior of a  $CACNA11$  variant [Murbartián et al., 2004] with different scalings (magenta:  $\epsilon = \frac{1}{2}$ , dark gray:  $\epsilon = \frac{1}{4}$ , cyan:  $\epsilon = -\frac{1}{4}$ , green:  $\epsilon = -\frac{1}{2}$ ). Inset: Zoomed-in view around the time of the spike. No notable differences between the variants and the control can be observed in the membrane potential time course. **C:** The  $[Ca^{2+}]$  response plotted in the phase plane for different variants. The behavior of variants of  $CACNA1C$  [Kudrnac et al., 2009],  $CACNB2$  [Link et al., 2009],  $CACNA11$  [Murbartián et al., 2004],  $ATP2B2$  [Empson et al., 2010],  $SCN1A$  [Cestèle et al., 2008], and  $KCNN3$  [Wittekindt et al., 2004] genes are shown with similar scaling as in (A) and (B).

this led to an increase in the SK current activation, relative to that in the control neuron. The increased  $I_{SK}$ , in turn, delayed the induction of the next spike, and hence resulted in a loss of gain (flattening) in the f-I curve (Figure 3). This finding is in line with previous modeling studies, which also have highlighted the role of  $Ca^{2+}$ -activated  $K^+$  currents in modulating f-I curves [Engel et al., 1999, Halmes et al., 2011].

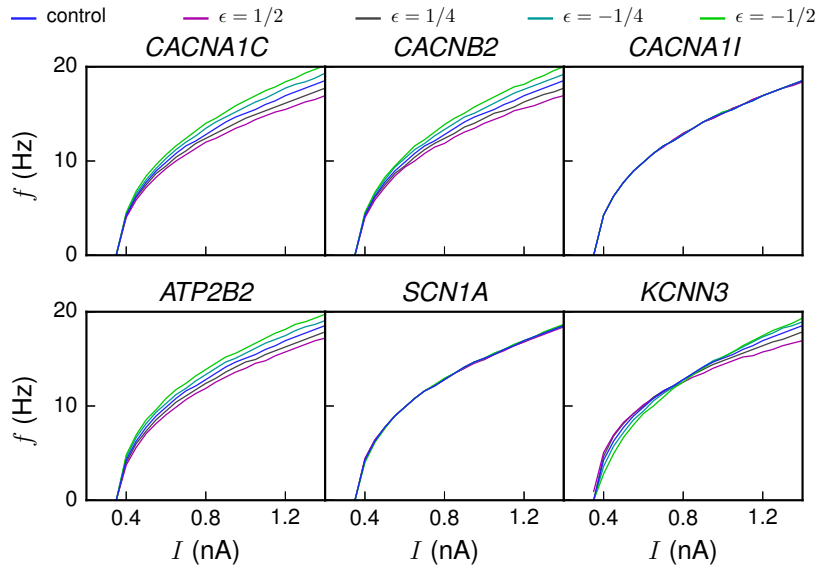


Figure 3: **The variant neurons show modulated gain.** f-I curves are shown for different scalings of different variants (magenta:  $\epsilon = \frac{1}{2}$ , dark gray:  $\epsilon = \frac{1}{4}$ , cyan:  $\epsilon = -\frac{1}{4}$ , green:  $\epsilon = -\frac{1}{2}$ ). Differences in gain are visible for  $CACNA1C$ ,  $CACNB2$ ,  $ATP2B2$ , and  $KCNN3$  variants.

We also studied the steady-state firing behavior by analyzing the limit cycle, i.e., the phase plane representation of the variable of interest after a large number of initial cycles. As the  $[Ca^{2+}]$  response served as the most sensitive biomarker, we used the  $[Ca^{2+}]$  limit cycle for this analysis. Figure 4 shows, for some of the gene variants, the  $[Ca^{2+}]$  limit cycle as a response to a long, square-pulse stimulus.

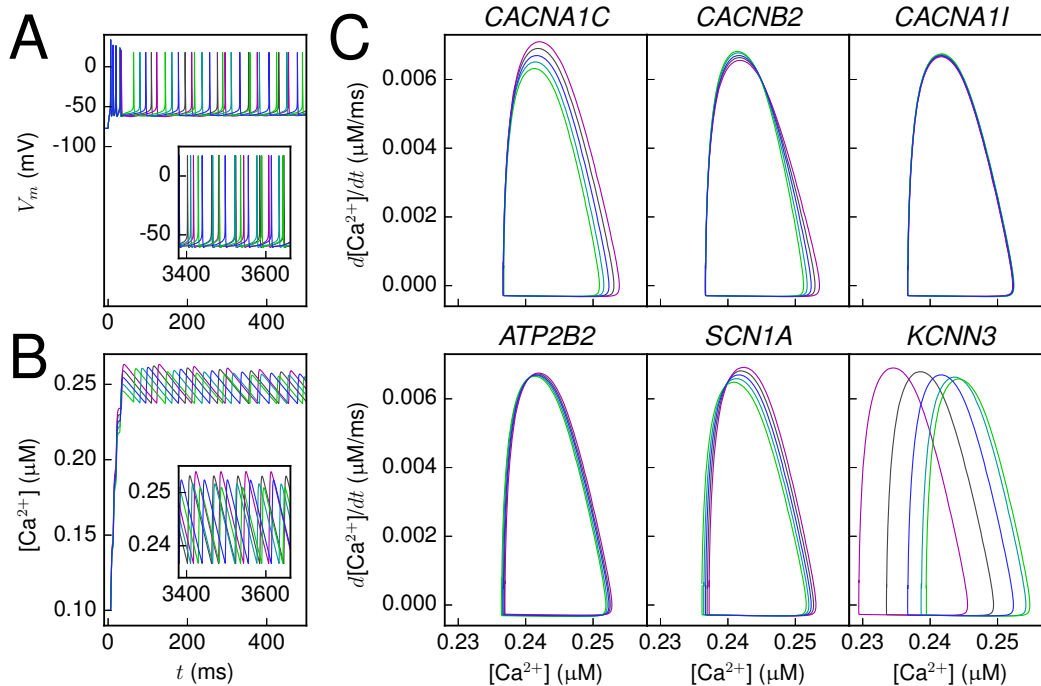


Figure 4: **Differences in  $[Ca^{2+}]$  limit cycles of the variants.** **A,B:** The membrane potential (A) and  $Ca^{2+}$  concentration (B) time courses at soma as a response to a DC with an amplitude of 1.2 nA. The different colors represent different scalings of a *CACNA1C* variant [Kudrnac et al., 2009] (scaling as in Figure 2). Inset: The time course shown 3.4 s since the beginning of the stimulus. **C:** The intracellular  $[Ca^{2+}]$  phase plane during steady firing caused by a DC applied to the soma. The variants and their scalings were chosen as in Figure 2C.

The different variants had different ways of impacting the shape of the  $[Ca^{2+}]$  limit cycle. An especially common trait was a shift or compression in the horizontal direction, representing a small increase or decrease of intracellular  $[Ca^{2+}]$  during steady firing. Figure S1 shows the range of  $[Ca^{2+}]$  values observed during the constant current injection for all variants used in this study. Interestingly, almost all variants gave deviations from the  $[Ca^{2+}]$  range observed in the control neuron.

The only genes that did not show notable variance for the range of  $[Ca^{2+}]$  during steady-state firing were *CACNA1I*, *KCNS3*, and *KCNB1*. Despite this, *CACNA1I* did have a clear effect on the  $[Ca^{2+}]$  phase plane in the single-pulse response (see Figure 2C). Conversely, the *KCNS3* and *KCNB1* variants were not found to influence any of the considered aspects of neuron behavior (see Figures S1 and S2). In these variants, the activation and inactivation of the persistent  $K^+$  current ( $I_{Kp}$ ) have been modified. Our findings reflect the overall minor role that the current  $I_{Kp}$  plays in shaping the response properties of the L5PC model neuron: It is only present in the soma and with relatively small maximal conductance [Hay et al., 2011]. The minor contribution of this current to the model neuron behavior may be in contradiction with experimental evidence, which states that this current constitutes a major proportion of the total outward  $K^+$  currents [Guan et al., 2007].

## Variants have an effect on integration of somatic and apical inputs

A question that arises from the observation of the above trends is whether, and to what extent, the small deviations from control neuron behavior affect the information processing capabilities of the neuron. In [Hay et al., 2011], it was shown that the L5PC model can be used to describe the  $Ca^{2+}$  spike generation as a response to a combination of stimuli at the apical dendrite and at the soma. Moreover, they showed a good qualitative match with experimental data and model predictions for the neuron responses during an “up” or “down” state. In this work, we followed their definition for the down state as the resting state of the neuron, and the up state as a state where a subthreshold current is applied to the proximal apical dendrite [Hay et al., 2011]. We also adopted their protocol of combining an apical and somatic stimulus and studying the effect of order and inter-stimulus interval (ISI) between the two (see Figure 8 in [Hay et al., 2011]). This gave us a temporal profile showing a range of ISI for which a large  $Ca^{2+}$  spike is produced. We then estimated the effect of our genetic variants on this temporal profile.

Figure 5 shows the temporal profiles for the six representative variants. Effects of the different variants on the

neuron response were visible both during the down and during the up state. Particularly large effects were observed in *CACNA1I* and *SCN1A* variants, which code for the LVA  $\text{Ca}^{2+}$  channels and transient  $\text{Na}^+$  channels that contribute to the sharp rise of voltage during an action potential. These channel types are expressed both in the soma and in the apical dendrite. Although all downscaled variants shared the basic form of the response curves, the shape was clearly altered in some variants. As shown in [Hay et al., 2011], the up-state temporal profile of the control neuron showed elevated apical responses when the apical stimulus was applied shortly after the somatic stimulus, but not when the apical stimulus was applied first. This order-specific response was changed in some of the variants (see e.g. *SCN1A* variant) so that they also produced large  $\text{Ca}^{2+}$  spikes when the apical stimulus was applied shortly before the somatic stimulus, and could hence alter the order sensitivity of the coincidence detection.

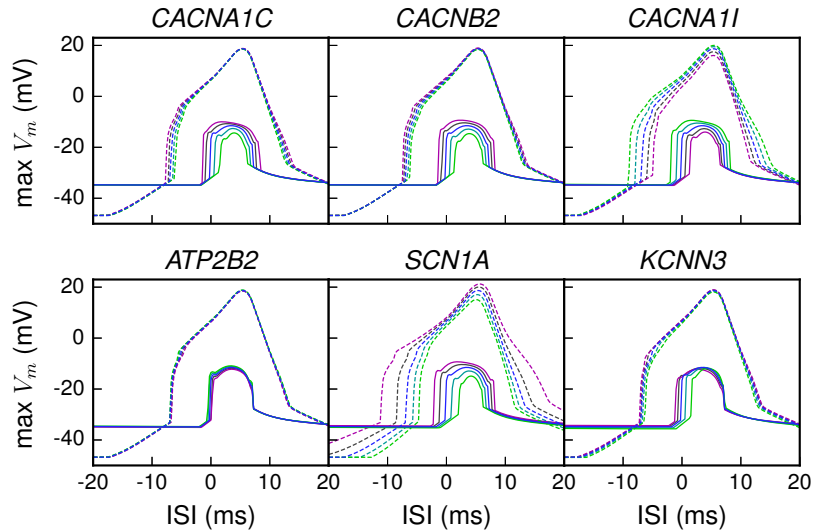


Figure 5: **Sensitivity of variant neurons to ISI between somatic and distal apical stimuli during up and down states.** The magnitude of the  $\text{Ca}^{2+}$  spikes was assessed by measuring the simulated membrane potential near the bifurcation point of the apical dendrite, i.e. at a distance of  $620 \mu\text{m}$  from the soma. The dashed lines show the temporal maximum of the model response membrane potential during a down state, and the solid lines during an up state. The x-axis represents the ISI between the somatic and apical stimuli, positive values denoting cases where the apical stimulus was applied after the somatic stimulus. The variants shown are the same as in Figure 2. In the up state paradigm, the neuron was first given a depolarizing square-pulse current of  $0.42 \text{ nA} \times 200 \text{ ms}$  at the proximal apical dendrite,  $200 \mu\text{m}$  from the soma. In the middle of this period, a somatic square-pulse current of  $0.5 \text{ nA} \times 5 \text{ ms}$  was applied, and after a time defined as the ISI, an alpha-shaped current injection with rise time  $0.5 \text{ ms}$ , decay time  $5 \text{ ms}$ , and maximal amplitude of  $0.5 \text{ nA}$  was applied. The down state paradigm was otherwise equal, but the long depolarizing current was absent, and to compensate this, the short somatic square-pulse current had an amplitude of  $1.8 \text{ nA}$ .

## Variants show differences in inhibition of a second apical stimulus

The alteration of information processing by the variants can also be seen in the sensitivity to successive synaptic inputs at the same locations. To explore this, we gave two successive stimuli to the apical dendrite, and varied the interval (ISI) between them. The first stimulus activated long time scale inhibitory currents, especially  $I_{SK}$  and  $I_m$ , and within some following time window, these currents could inhibit the generation of a subsequent spike. This could be interpreted as a form of single-cell pre-pulse inhibition: If the initial input caused the neuron to spike, the next input could fail to do so, even at times when the second stimulus were of larger amplitude.

Figure 6 shows how the threshold synaptic conductance needed for inducing a second spike, relative to the one needed for the first spike, depends on the ISI. Interestingly, the threshold conductance curve was affected by many of the variants, especially by the variants of  $\text{Ca}^{2+}$  channel genes. Although the shown effect was partly attributed to the differences in the spiking thresholds between the variants, differences between the variants could still be observed when an absolute spiking threshold values for inducing a second spike were considered (data not shown). These findings raise the possibility that the disturbed prepulse inhibition observed in many SCZ patients might be an effect of altered ionic channel properties at the single neuron level, and not only of the modified elements in synaptic circuitry as previously thought [Swerdlow and Geyer, 1993, Medan and Preuss, 2011] (cf. [Koch, 2012]).

## Combinations of variants may cause large alterations of neuron excitability

The effects of the variants on neuron excitability, as explored in Figures 2–6, were relatively small when the variants were studied in isolation (this was also the intention behind the downscaling process). However, combinations of



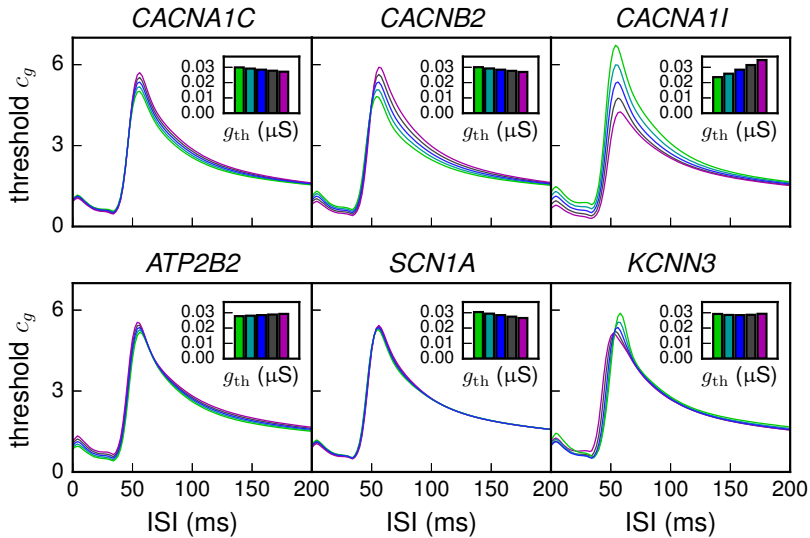


Figure 6: **Threshold conductance factor for inducing a second spike as a function of ISI.** The neuron was first made to spike by applying 3000 simultaneously activated synaptic conductances that were uniformly distributed along the apical dendrite at a distance [300  $\mu\text{m}$ , 1300  $\mu\text{m}$ ] from the soma. All synaptic conductances were alpha-shaped with  $\tau = 5$  ms and maximal conductance  $1.1g_{\text{th}}$ , where  $g_{\text{th}}$  was the threshold conductance value for inducing a spike in resting state. These values were variant-specific (and scaling-specific), and they are plotted in the inset of each panel. After the specified ISI, the synapses were activated again. The  $y$ -axis shows the factor  $c_g$ , chosen such that  $c_g g_{\text{th}}$  was the threshold conductance of the second stimulus for generating an extra spike. Curves above the control curve (blue) represent strengthened prepulse inhibition, while curves below it represent weakened prepulse inhibition. The effect of the *KCNN3* variant ( $\epsilon = \frac{1}{2}$ , magenta) was bilateral: For  $\text{ISI} \lesssim 50$  ms, the effect was strengthening, whereas for  $\text{ISI} \gtrsim 50$  ms, the effect was weakening.

variants of different genes may have additive effects on the neuron excitability. As a final step of our inquiry, we went on to investigate the effect that combinations of several of the variants could have. Figure S3 shows a selected example of how a combination of variants altered the neuron firing properties considered in Figures 2–6. Although this version of the model neuron consists of downscaled variants, the properties of neuron excitability were remarkably modified.

## Discussion

We presented a framework for studying the effects of genetic variants in genes related to schizophrenia (SCZ) on layer V pyramidal cell (L5PC) excitability. Our results indicate that most of the studied variants predict an observable change in the neuron behavior (see Figures 2–6). Taken together, these data provide support for using neuronal modeling to study the functional implications of SCZ-related genes on neuronal excitability. Although the analyses presented in this paper are specific to L5PCs and SCZ-related genes, our framework may be directly applicable to other cell types and other polygenic diseases, such as bipolar disorder and autism, given an identification of risk genes related to neuronal excitability. Furthermore, our approach can be directly extended to biophysically detailed models of neuronal networks, e.g. [Hay and Segev, 2014].

The results shown in the present paper are based on a multi-compartmental neuron model [Hay et al., 2011] employing a certain set of ionic channels. Alternative models with comparable complexity have recently been published. The authors of [Bahl et al., 2012] present and apply a method for fitting the L5PC model to a simplified neuron morphology. In another recent work [Almog and Korngreen, 2014], the L5PC model was fit to each stained morphology and the corresponding recordings separately. To rule out our conclusions being an artefact of a certain specific morphology, we carried out our analyses on another neuron model fit (cell #1 equipped with channel conductance values from the first column of Table S1 in [Hay et al., 2011]) and an alternative neuron morphology (cell #2 of [Hay et al., 2011]). The trend of the variant effects remained the same in these simulations (see Supplemental information, Figures S4 and S5). More comprehensive analysis could be carried out by using the above-mentioned alternative models, or by employing a wider set of neuron morphologies [Hay et al., 2013], but this is left for future work.

Discovering the disease mechanisms of disorders with polygenic architecture, such as SCZ, requires considering the interplay between many different biological processes and entities. The computational framework presented here allows one to identify physiological mechanisms and biomarkers common across multiple risk-related genes. Although there are many more SCZ-related genes [Ripke et al., 2014] than those listed in Table 1, the identified variants capture multiple types of changes in neuron excitability (see Figures 2–6). This allows studying the effects of combinations of different genetic variants in a straightforward manner, as suggested in Supplemental information (Figure S3), although

one should be careful in the interpretation of the results as certain variants could have non-additive effects. The gene hits not considered in the present work contribute to e.g. expression level and function of ionotropic and G-protein coupled receptors, as well as phosphorylation and dephosphorylation of diverse proteins. It should be noted that several of the identified SCZ-related genes, such as *PTN*, *PAK6*, and *SNAP91* may also affect neuron morphology [Deuel et al., 2002, Nekrasova et al., 2008, Ang et al., 2003, Dickman et al., 2006]. Our framework could be extended to include some of these effects, but studying the contribution of many signaling genes is out of the scope of the used neuron model.

Linking cellular mechanisms to SCZ can be extremely difficult due to the high cognitive level on which the disease symptoms usually emerge. There is however one important exception, namely, altered prepulse inhibition, which is found in approximately 40-50% of SCZ patients [Turetsky et al., 2007]. In the present study, we showed that the considered genetic variants may have different tendencies to suppress a second synaptic stimulus, owing only to the differences in the (non-synaptic) ion channel gating or  $\text{Ca}^{2+}$  dynamics (Figure 6). This could be an important contributor to understanding the phenomenon of prepulse inhibition, although deficiencies in synaptic connections are most likely to play a role as well [Swerdlow and Geyer, 1993]. Moreover, altered integration of local and distal inputs in the manner of Figure 5 could possibly underlie incomplete or excessive activation of pyramidal cells in certain brain areas linked to auditory hallucinations ([Larkum, 2013]; see also discussion of the role of spontaneous activity in primary auditory cortex in triggering verbal hallucinations in [Kompus et al., 2013]). Experimental testing of the shown model predictions for integration of inputs on a single-cell level is possible as well. Even without genetic manipulations, the downscaled variants of the ion channels could be imitated *in vitro* by partial pharmacological blocks that are configured to cause changes in currents comparable to those in our variants. However, in such a case the fine details on e.g. current activation time constants would be dismissed.

The genetic variation of ion channels will affect not only the membrane potentials of the neurons, but also the transmembrane currents generating the local field potential (LFP) recorded inside cortex and the electrocorticography (ECoG) signals recorded at the cortical surface [Buzsáki et al., 2012, Einevoll et al., 2013]. Further, the same transmembrane currents also determine the neuronal current dipole moments measured in EEG and MEG [Nunez and Srinivasan, 2006, Hämäläinen et al., 1993]. Thus a natural extension of the present work is to investigate the effects of the genetic variation of the single-neuron current dipole moments [Lindén et al., 2010] and the corresponding single-neuron contribution to the EEG signals. This is left for future work.

A severe limitation of our approach is the lack of data on how different specific SCZ-related genetic polymorphisms affect the ion channel function and  $\text{Ca}^{2+}$  dynamics. In this paper, we used literature data on extreme variants (e.g., loss of function mutations) of the identified SCZ-related risk genes, from a range of cell types, including non-neural tissues. Ideally, one would want to use physiological measures for the relevant genetic variants in the actual cell types (i.e., L5PCs) in cortical circuits, but such data do not currently exist. On the other hand, the diversity of data in the literature that we used and the possible discrepancies in the experimental procedures therein could also reflect in the results shown in this study, although our downscaling procedure constrains such errors from above. Novel methods employing automated cell patching [Ranjan et al., 2014] to test the effects of subtle SCZ-related SNPs could provide the solution to both above limitations of our study.

The validity of the downscaling, which for the aforementioned reasons is a central procedure in our framework, is built upon two assumptions: 1) That the SCZ-related gene variants do affect neuronal excitability on a single-neuron level, and 2) that their effects on ion channel or calcium pump kinetics are smaller than those of certain already documented mutations with extreme phenotypic consequences, such as deafness, hemiplegic migraine, or other pain disorders. The first assumption can be argued for by the multitude of ion channel-encoding genes that have been shown to be related to SCZ risk, and the second by the lack of severe body malfunctioning (such as the abovementioned ones) in SCZ patients, but rigorous proofs for both assumptions are yet to be shown. A challenge for future studies is also to decipher how the ion channel densities are affected by the variants in various cell types, an issue that might be important in modeling the effects of SCZ-associated polymorphisms.

Our framework is an early attempt toward understanding the disease mechanisms of polygenic psychiatric disorders by computational means. It binds together genetic and single neuron levels of abstraction in the big picture of modeling psychiatric illnesses, as recently sketched in [Wang and Krystal, 2014] and [Corlett and Fletcher, 2014]. While earlier computational studies considered only effects of single variants on neuron firing behavior [Murbartián et al., 2004, Zhang et al., 2011], our framework allows the screening of multiple types of variants and their implications on the neuron excitability. It may serve as a proof of principle for a novel “Biophysical Psychiatry” approach, enabling the integration of information from previously disparate fields of study including GWASs, functional genomics, and biophysical computational modeling using models of moderate complexity. We consider the chosen level of complexity a suitable trade-off for this purpose: While more approximate models, such as integrate-and-fire models, could not distinguish between the effects of different genetic variants in an acceptable precision, more detailed models including e.g. dynamics of protein translation and phosphorylation are likely to be very computation-intensive. The challenge for future work is to extend the study to both larger and finer spatial and temporal scales.

## Acknowledgements

NOTUR resources (NN4661K, NN9114K, NS9114K) were used for heavy simulations. Funding: NIH grant 5 R01 EB000790-10, EC-FP7 grant 604102 (“Human Brain Project”), Research Council of Norway (216699, 213837 and 223273), South East Norway Health Authority (2013-123), and KG Jebsen Foundation.

## Financial disclosures

The authors declare that there are no conflicts of interest.

## Author contributions

Designed the study: TMM, GTE, OAA, AMD. Provided data or analytical support: SD, GH, AD, YW, GTE, AMD. Performed the analysis: TMM. Interpreted the results: TMM, GH, AD, AW, FB, SD, YW, GTE, OAA, AMD. Wrote the manuscript: TMM, GH, AD, GTE, OAA, AMD.

## References

- [Almog and Korngreen, 2014] Almog, M. and Korngreen, A. (2014). A quantitative description of dendritic conductances and its application to dendritic excitation in layer 5 pyramidal neurons. *J Neurosci*, 34(1):182–196.
- [Ang et al., 2003] Ang, L.-H., Kim, J., Stepensky, V., and Hing, H. (2003). Dock and Pak regulate olfactory axon pathfinding in *Drosophila*. *Development*, 130(7):1307–1316.
- [Bahl et al., 2012] Bahl, A., Stemmler, M. B., Herz, A. V., and Roth, A. (2012). Automated optimization of a reduced layer 5 pyramidal cell model based on experimental data. *J Neurosci Met*, 210(1):22–34.
- [Bock et al., 2011] Bock, G., Gebhart, M., Scharinger, A., Jangsangthong, W., Busquet, P., Poggiani, C., Sartori, S., Mangoni, M. E., Sinnegger-Brauns, M. J., Herzig, S., et al. (2011). Functional properties of a newly identified c-terminal splice variant of *cav1.3* l-type  $ca^{2+}$  channels. *J Biol Chem*, 286(49):42736–42748.
- [Bocksteins et al., 2011] Bocksteins, E., Ottshytsch, N., Timmermans, J.-P., Labro, A., and Snyders, D. (2011). Functional interactions between residues in the S1, S4, and S5 domains of Kv2.1. *Eur Biophys J*, 40(6):783–793.
- [Buzsáki et al., 2012] Buzsáki, G., Anastassiou, C. A., and Koch, C. (2012). The origin of extracellular fields and currents—eeg, ecog, lfp and spikes. *Nat Rev Neurosci*, 13(6):407–420.
- [Cestèle et al., 2008] Cestèle, S., Scalmani, P., Rusconi, R., Terragni, B., Franceschetti, S., and Mantegazza, M. (2008). Self-limited hyperexcitability: Functional effect of a familial hemiplegic migraine mutation of the Nav1.1 (SCN1A)  $na^{+}$  channel. *J Neurosci*, 28(29):7273–7283.
- [Cordeiro et al., 2009] Cordeiro, J. M., Marieb, M., Pfeiffer, R., Calloe, K., Burashnikov, E., and Antzelevitch, C. (2009). Accelerated inactivation of the L-type calcium current due to a mutation in CACNB2b underlies brugada syndrome. *J Mol Cell Cardiol*, 46(5):695–703.
- [Corlett and Fletcher, 2014] Corlett, P. R. and Fletcher, P. C. (2014). Computational psychiatry: A Rosetta Stone linking the brain to mental illness. *Lancet Psychiatry*, 1(5):399–402.
- [Deuel et al., 2002] Deuel, T. F., Zhang, N., Yeh, H.-J., Silos-Santiago, I., and Wang, Z.-Y. (2002). Pleiotrophin: A cytokine with diverse functions and a novel signaling pathway. *Arch Biochem Biophys*, 397(2):162–171.
- [Dib-Hajj et al., 2005] Dib-Hajj, S., Rush, A., Cummins, T., Hisama, F., Novella, S., Tyrrell, L., Marshall, L., and Waxman, S. (2005). Gain-of-function mutation in *nav1.7* in familial erythromelalgia induces bursting of sensory neurons. *Brain*, 128(8):1847–1854.
- [Dickman et al., 2006] Dickman, D. K., Lu, Z., Meinertzhagen, I. A., and Schwarz, T. L. (2006). Altered synaptic development and active zone spacing in endocytosis mutants. *Curr Biol*, 16(6):591–598.
- [Einevoll et al., 2013] Einevoll, G. T., Kayser, C., Logothetis, N. K., and Panzeri, S. (2013). Modelling and analysis of local field potentials for studying the function of cortical circuits. *Nat Rev Neurosci*, 14(11):770–785.
- [Empson et al., 2010] Empson, R. M., Akemann, W., and Knöpfel, T. (2010). The role of the calcium transporter protein plasma membrane calcium ATPase PMCA2 in cerebellar Purkinje neuron function. *Funct Neurol*, 25(3):153.

- [Engel et al., 1999] Engel, J., Schultens, H. A., and Schild, D. (1999). Small conductance potassium channels cause an activity-dependent spike frequency adaptation and make the transfer function of neurons logarithmic. *Biophys J*, 76(3):1310–1319.
- [Estacion et al., 2008] Estacion, M., Dib-Hajj, S., Benke, P., te Morsche, R. H., Eastman, E., Macala, L., Drenth, J., and Waxman, S. (2008). Nav1.7 gain-of-function mutations as a continuum: A1632e displays physiological changes associated with erythromelalgia and paroxysmal extreme pain disorder mutations and produces symptoms of both disorders. *J Neurosci*, 28(43):11079–11088.
- [Estacion et al., 2011] Estacion, M., Han, C., Choi, J.-S., Hoeijmakers, J., Lauria, G., Drenth, J., Gerrits, M. M., Dib-Hajj, S. D., Faber, C. G., Merkies, I., et al. (2011). Intra- and interfamily phenotypic diversity in pain syndromes associated with a gain-of-function variant of nav1.7. *Mol Pain*, 7:92.
- [Fakira et al., 2012] Fakira, A. K., Gaspers, L. D., Thomas, A. P., Li, H., Jain, M. R., and Elkabes, S. (2012). Purkinje cell dysfunction and delayed death in plasma membrane calcium atpase 2-heterozygous mice. *Mol Cell Neurosci*, 51(1):22–31.
- [Ficarella et al., 2007] Ficarella, R., Di Leva, F., Bortolozzi, M., Ortolano, S., Donaudy, F., Petrillo, M., Melchionda, S., Lelli, A., Domi, T., Fedrizzi, L., et al. (2007). A functional study of plasma-membrane calcium-pump isoform 2 mutants causing digenic deafness. *Proc Natl Acad Sci*, 104(5):1516–1521.
- [Fromer et al., 2014] Fromer, M., Pocklington, A. J., Kavanagh, D. H., Williams, H. J., Dwyer, S., Gormley, P., Georgieva, L., Rees, E., Palta, P., Ruderfer, D. M., Carrera, N., Humphreys, I., Johnson, J. S., Roussos, P., Barker, D. D., Banks, E., Milanova, V., Grant, S. G., Hannon, E., Rose, S. A., Chambert, K., Mahajan, M., Scolnick, E. M., Moran, J. L., Kirov, G., Palotie, A., McCarroll, S. A., Holmans, P., Sklar, P., Owen, M. J., Purcell, S. M., and O’Donovan, M. C. (2014). De novo mutations in schizophrenia implicate synaptic networks. *Nature*, 506(7487):179–184.
- [Gottesman and Shields, 1967] Gottesman, I. I. and Shields, J. (1967). A polygenic theory of schizophrenia. *Proc Natl Acad Sci*, 58(1):199.
- [Grillner, 2014] Grillner, S. (2014). Megascience efforts and the brain. *Neuron*, 82(6):1209–1211.
- [Guan et al., 2007] Guan, D., Tkatch, T., Surmeier, D., Armstrong, W., and Foehring, R. (2007). Kv2 subunits underlie slowly inactivating potassium current in rat neocortical pyramidal neurons. *J Physiol*, 581(3):941–960.
- [Halmes et al., 2011] Halmes, G., Augustinaite, S., Heggelund, P., Einevoll, G. T., and Migliore, M. (2011). A multi-compartment model for interneurons in the dorsal lateral geniculate nucleus. *PLoS Comput Biol*, 7:e1002160.
- [Hämäläinen et al., 1993] Hämäläinen, M., Hari, R., Ilmoniemi, R. J., Knuutila, J., and Lounasmaa, O. V. (1993). Magnetoencephalography—theory, instrumentation, and applications to noninvasive studies of the working human brain. *Rev Mod Phys*, 65:413–497.
- [Han et al., 2006] Han, C., Rush, A. M., Dib-Hajj, S. D., Li, S., Xu, Z., Wang, Y., Tyrrell, L., Wang, X., Yang, Y., and Waxman, S. G. (2006). Sporadic onset of erythromelalgia: A gain-of-function mutation in nav1.7. *Ann Neurol*, 59(3):553–558.
- [Hay et al., 2011] Hay, E., Hill, S., Schürmann, F., Markram, H., and Segev, I. (2011). Models of neocortical layer 5b pyramidal cells capturing a wide range of dendritic and perisomatic active properties. *PLoS Comput Biol*, 7:e1002107.
- [Hay et al., 2013] Hay, E., Schürmann, F., Markram, H., and Segev, I. (2013). Preserving axosomatic spiking features despite diverse dendritic morphology. *J Neurophysiol*, 109(12):2972–2981.
- [Hay and Segev, 2014] Hay, E. and Segev, I. (2014). Dendritic excitability and gain control in recurrent cortical microcircuits. *Cerebral Cortex*, page bhu200.
- [Ishii et al., 2007] Ishii, T. M., Nakashima, N., and Ohmori, H. (2007). Tryptophan-scanning mutagenesis in the s1 domain of mammalian hcn channel reveals residues critical for voltage-gated activation. *J Physiol*, 579(2):291–301.
- [Ji et al., 2000] Ji, Y., Lalli, M. J., Babu, G. J., Xu, Y., Kirkpatrick, D. L., Liu, L. H., Chiamvimonvat, N., Walsh, R. A., Shull, G. E., and Periasamy, M. (2000). Disruption of a single copy of the serca2 gene results in altered ca2+ homeostasis and cardiomyocyte function. *J Biol Chem*, 275(48):38073–38080.
- [Koch, 2012] Koch, M. (2012). Clinical relevance of animal models of schizophrenia. *Suppl Clin Neurophysiol*, 62:113–120.

- [Kompus et al., 2013] Kompus, K., Falkenberg, L. E., Bless, J. J., Johnsen, E., Kroken, R. A., Kråkvik, B., Larøi, F., Løberg, E.-M., Vedul-Kjelsås, E., Westerhausen, R., et al. (2013). The role of the primary auditory cortex in the neural mechanism of auditory verbal hallucinations. *Front Hum Neurosci*, 7:144.
- [Kudrnac et al., 2009] Kudrnac, M., Beyl, S., Hohaus, A., Stary, A., Peterbauer, T., Timin, E., and Hering, S. (2009). Coupled and independent contributions of residues in IS6 and IIS6 to activation gating of CaV1.2. *J Biol Chem*, 284(18):12276–12284.
- [Larkum, 2013] Larkum, M. (2013). A cellular mechanism for cortical associations: An organizing principle for the cerebral cortex. *Trends Neurosci*, 36(3):141–151.
- [Lee et al., 2012] Lee, S. H., DeCandia, T. R., Ripke, S., Yang, J., Sullivan, P. F., Goddard, M. E., Keller, M. C., Visscher, P. M., Wray, N. R., Schizophrenia Psychiatric Genome-Wide Association Study Consortium, et al. (2012). Estimating the proportion of variation in susceptibility to schizophrenia captured by common snps. *Nat Gen*, 44(3):247–250.
- [Lindén et al., 2010] Lindén, H., Pettersen, K. H., and Einevoll, G. T. (2010). Intrinsic dendritic filtering gives low-pass power spectra of local field potentials. *J Comput Neurosci*, 29(3):423–444.
- [Link et al., 2009] Link, S., Meissner, M., Held, B., Beck, A., Weissgerber, P., Freichel, M., and Flockerzi, V. (2009). Diversity and developmental expression of L-type calcium channel  $\beta 2$  proteins and their influence on calcium current in murine heart. *J Biol Chem*, 284(44):30129–30137.
- [Massa et al., 1995] Massa, E., Kelly, K. M., Yule, D. I., MacDonald, R. L., and Uhler, M. D. (1995). Comparison of fura-2 imaging and electrophysiological analysis of murine calcium channel alpha 1 subunits coexpressed with novel beta 2 subunit isoforms. *Mol Pharmacol*, 47(4):707–716.
- [Medan and Preuss, 2011] Medan, V. and Preuss, T. (2011). Dopaminergic-induced changes in mauthner cell excitability disrupt prepulse inhibition in the startle circuit of goldfish. *J Neurophysiol*, 106(6):3195–3204.
- [Murbartián et al., 2004] Murbartián, J., Arias, J. M., and Perez-Reyes, E. (2004). Functional impact of alternative splicing of human T-type Cav3.3 calcium channels. *J Neurophysiol*, 92(6):3399–3407.
- [Nekrasova et al., 2008] Nekrasova, T., Jobes, M. L., Ting, J. H., Wagner, G. C., and Minden, A. (2008). Targeted disruption of the pak5 and pak6 genes in mice leads to deficits in learning and locomotion. *Dev Biol*, 322(1):95–108.
- [Nunez and Srinivasan, 2006] Nunez, P. L. and Srinivasan, R. (2006). *Electric fields of the brain: the neurophysics of EEG*. Oxford university press.
- [Owen, 2014] Owen, M. J. (2014). New approaches to psychiatric diagnostic classification. *Neuron*, 84(3):564–571.
- [Pérez-Alvarez et al., 2011] Pérez-Alvarez, A., Hernández-Vivanco, A., Caba-González, J. C., and Albillos, A. (2011). Different roles attributed to cav1 channel subtypes in spontaneous action potential firing and fine tuning of exocytosis in mouse chromaffin cells. *J Neurochem*, 116(1):105–121.
- [Purcell et al., 2009] Purcell, S. M., Wray, N. R., Stone, J. L., Visscher, P. M., O’Donovan, M. C., Sullivan, P. F., Sklar, P., Purcell, S. M., Stone, J. L., Sullivan, P. F., et al. (2009). Common polygenic variation contributes to risk of schizophrenia and bipolar disorder. *Nature*, 460(7256):748–752.
- [Ranjan et al., 2014] Ranjan, R., Logette, E., Petitprez, S., Marani, M., Mirjia, H., Muller, E. B., Schuermann, F., and Markram, H. (2014). Automated biophysical characterization of the complete rat Kv-ion channel family. Society for Neuroscience Meeting (SfN 2014), Washington, DC, USA, November 15-19, 2014.
- [Ripke et al., 2014] Ripke, S., Neale, B. M., Corvin, A., Walters, J. T., Farh, K. H., Holmans, P., Lee, P., Bulik-Sullivan, B., Collier, D. A., Huang, H., Pers, T., Agartz, I., Agerbo, E., Albus, M., Alexander, M., Amin, F., et al. (2014). Biological insights from 108 schizophrenia-associated genetic loci. *Nature*, 511(7510):421–427.
- [Ripke et al., 2013] Ripke, S., O’Dushlaine, C., Chambert, K., Moran, J. L., Kähler, A. K., Akterin, S., Bergen, S. E., Collins, A. L., Crowley, J. J., Fromer, M., et al. (2013). Genome-wide association analysis identifies 13 new risk loci for schizophrenia. *Nat Gen*, 45(10):1150–1159.
- [Ripke et al., 2011] Ripke, S., Sanders, A. R., Kendler, K. S., Levinson, D. F., Sklar, P., Holmans, P. A., Lin, D. Y., Duan, J., Ophoff, R. A., A., A. O., Scolnick, E., et al. (2011). Genome-wide association study identifies five new schizophrenia loci. *Nat Gen*, 43(10):969–976.
- [Shepard and Rae, 1999] Shepard, A. R. and Rae, J. L. (1999). Electrically silent potassium channel subunits from human lens epithelium. *Am J Physiol-Cell Ph*, 277(3):C412–C424.

- [Sklar et al., 2011] Sklar, P., Ripke, S., Scott, L. J., Andreassen, O. A., Cichon, S., Craddock, N., Edenberg, H. J., Nurnberger, J. I., Rietschel, M., Blackwood, D., et al. (2011). Large-scale genome-wide association analysis of bipolar disorder identifies a new susceptibility locus near ODZ4. *Nat Gen*, 43(10):977.
- [Smoller et al., 2013] Smoller, J., Ripke, S., Lee, P., Neale, B., Nurnberger, J., Santangelo, S., Sullivan, P., Perlis, R., Purcell, S., Fanous, A., and Neale, M. (2013). Identification of risk loci with shared effects on five major psychiatric disorders: A genome-wide analysis. *Lancet*, 381(9875):1371.
- [Stefansson et al., 2009] Stefansson, H., Ophoff, R. A., Steinberg, S., Andreassen, O. A., Cichon, S., Rujescu, D., Werge, T., Pietiläinen, O. P., Mors, O., Mortensen, P. B., et al. (2009). Common variants conferring risk of schizophrenia. *Nature*, 460(7256):744–747.
- [Swerdlow and Geyer, 1993] Swerdlow, N. and Geyer, M. (1993). Prepulse inhibition of acoustic startle in rats after lesions of the pedunculopontine tegmental nucleus. *Beh Neurosci*, 107(1):104.
- [Tan et al., 2011] Tan, B. Z., Jiang, F., Tan, M. Y., Yu, D., Huang, H., Shen, Y., and Soong, T. W. (2011). Functional characterization of alternative splicing in the c terminus of l-type cav1.3 channels. *J Biol Chem*, 286(49):42725–42735.
- [Turetsky et al., 2007] Turetsky, B. I., Calkins, M. E., Light, G. A., Olincy, A., Radant, A. D., and Swerdlow, N. R. (2007). Neurophysiological endophenotypes of schizophrenia: the viability of selected candidate measures. *Schizophr Bull*, 33(1):69–94.
- [van Os and Kapur, 2009] van Os, J. and Kapur, S. (2009). Schizophrenia. *Lancet*, 374(9690):635–645.
- [Vanmolkot et al., 2007] Vanmolkot, K. R., Babini, E., de Vries, B., Stam, A. H., Freilinger, T., Terwindt, G. M., Norris, L., Haan, J., Frants, R. R., Ramadan, N. M., et al. (2007). The novel p.L1649Q mutation in the SCN1A epilepsy gene is associated with familial hemiplegic migraine: genetic and functional studies. *Hum Mutat*, 28(5):522–522.
- [Wang and Krystal, 2014] Wang, X.-J. and Krystal, J. H. (2014). Computational psychiatry. *Neuron*, 84(3):638–654.
- [Wen et al., 2014] Wen, Z., Nguyen, H. N., Guo, Z., Lalli, M. A., Wang, X., Su, Y., Kim, N.-S., Yoon, K.-J., Shin, J., Zhang, C., et al. (2014). Synaptic dysregulation in a human ipsc cell model of mental disorders. *Nature*, 515:414–418.
- [Wittekindt et al., 2004] Wittekindt, O. H., Visan, V., Tomita, H., Imtiaz, F., Gargus, J. J., Lehmann-Horn, F., Grissmer, S., and Morris-Rosendahl, D. J. (2004). An apamin- and scyllatoxin-insensitive isoform of the human SK3 channel. *Mol Pharmacol*, 65(3):788–801.
- [Zhang et al., 2011] Zhang, Q., Timofeyev, V., Qiu, H., Lu, L., Li, N., Singapuri, A., Torado, C. L., Shin, H. S., and Chiamvimonvat, N. (2011). Expression and roles of Cav1.3 ( $\alpha 1D$ ) L-type  $Ca^{2+}$  channel in atrioventricular node automaticity. *J Mol Cell Cardiol*, 50(1):194–202.

# Functional effects of schizophrenia-linked genetic variants on intrinsic single-neuron excitability: A modeling study. Supplemental information

## Methods

### The L5PC model

The current balance equation for each compartment of the neuron can be written as

$$C_m \frac{\partial V}{\partial t} = I_{Nat} + I_{Nap} + I_h + I_m + I_{Kp} + I_{Kt} + I_{Kv3.1} + I_{CaHVA} + I_{CaLVA} + I_{SK} + I_l + I_{axial},$$

where each type of current, except for the axial current, can be described as a multiplication of activation and inactivation variables as

$$I = \bar{g} m^{N_m} h^{N_h} (E - V).$$

Here,  $\bar{g}$  is the maximal conductance of the ion channels,  $m$  and  $h$  are the activation and inactivation variables while  $N_m$  and  $N_h$  are constants describing their sensitivities, and  $E$  is the reversal potential corresponding to the ionic species. Reversal potentials of  $\text{Na}^+$  and  $\text{K}^+$  are constants ( $E_{Na} = 50$  mV,  $E_K = -85$  mV), while the reversal potential of  $\text{Ca}^{2+}$  depends on the intracellular  $[\text{Ca}^{2+}]$ :  $E_{Ca}$  varied between 96 mV and 120 mV in our simulations. The dynamics of the activation and inactivation variables are defined as

$$\frac{dm}{dt} = \frac{m - m_\infty}{\tau_m} \quad \text{and} \quad \frac{dh}{dt} = \frac{h - h_\infty}{\tau_h},$$

where  $m_\infty$ ,  $h_\infty$ ,  $\tau_m$ , and  $\tau_h$  are functions of membrane potential  $V$ . Typically, functions  $m_\infty$  and  $h_\infty$  have a sigmoidal shape, where the half-activation and half-inactivation voltages are determined by one or more (depending on ion channel) parameters each. We denote these parameters  $V_{\text{offm}^*}$  and  $V_{\text{offh}^*}$ , where  $*$  stands for further specifications if there are multiple parameters affecting the half-(in)activation voltage. In a similar fashion, parameters  $V_{\text{slo}m^*}$  and  $V_{\text{slo}h^*}$  affect the slopes of the (in)activation curves, and parameters  $\tau_{\text{m}^*}$  and  $\tau_{\text{offh}^*}$  influence the time constants. As an exception, the activation of  $I_{SK}$  is solely dependent on the intracellular  $[\text{Ca}^{2+}]$ , and this dependence is quantified by half-activation concentration parameter  $c_{\text{off}}$  and slope parameter  $c_{\text{slo}}$ . The intracellular  $[\text{Ca}^{2+}]$  obeys the following dynamics:

$$\frac{d[\text{Ca}^{2+}]_i}{dt} = \frac{I_{CaHVA} + I_{CaLVA}}{2\gamma Fd} - \frac{[\text{Ca}^{2+}]_i - c_{\text{min}}}{\tau_{\text{decay}}},$$

where  $I_{CaHVA}$  and  $I_{CaLVA}$  are the high and low-voltage activated  $\text{Ca}^{2+}$  currents entering the considered cell segment,  $\gamma$  represents the fraction of  $\text{Ca}^{2+}$  ions entering the cell that contribute to the intracellular  $[\text{Ca}^{2+}]$ ,  $F$  the Faraday constant,  $d$  is the depth of the sub-membrane layer considered for calculation of concentration,  $c_{\text{min}}$  the resting intracellular  $[\text{Ca}^{2+}]$ , and  $\tau_{\text{decay}}$  is the decay time constant of the intracellular  $[\text{Ca}^{2+}]$ . The simulation codes are provided in the ModelDB entry 169457 (<https://senselab.med.yale.edu/ModelDB>).

### Channel activation and inactivation dynamics

Here, the model equations and parameter values are listed for all ion channels. The maximal conductances  $\bar{g}$  are different for different parts of the neuron: The subindex  $s$  refers to soma,  $ad$  to apical dendrite,  $bd$  to basal dendrite, and  $ax$  to axon, and for each current type all unshown maximal conductances are zero. For the non-specific ionic currents and  $\text{Ca}^{2+}$  currents, the maximal conductances vary spatially along the apical dendrite in the following way. In the ‘‘hot zone’’, which lies on the distance 650 $\mu\text{m}$ –850 $\mu\text{m}$ , the maximal conductances of  $\text{Ca}^{2+}$  currents are ten or hundredfold larger than elsewhere in the apical dendrite. The maximal conductances of the non-specific ionic current in turn grow exponentially from 0 to the length of the longest branch,  $L_{\text{max}}$ , which is 1300  $\mu\text{m}$  in this study. The numerical values correspond to the control neuron values and may be varied in the variant neurons.

#### Fast inactivating $\text{Na}^+$ current, $I_{Nat}$

$$\alpha_m = -\frac{1}{\tau_{\text{ma}}} \cdot \frac{V_{\text{offm}} - V}{1 - \exp\left(\frac{(V_{\text{offm}} - V)}{V_{\text{slo}m}}\right)}$$

$$\beta_m = \frac{1}{\tau_{mb}} \cdot \frac{V_{\text{offm}} - V}{1 - \exp\left(\frac{-(V_{\text{offm}} - V)}{V_{\text{slo m}}}\right)}$$

$$\alpha_h = \frac{1}{\tau_{ha}} \cdot \frac{V_{\text{offh}} - V}{1 - \exp\left(\frac{(V_{\text{offh}} - V)}{V_{\text{sloh}}}\right)}$$

$$\beta_h = -\frac{1}{\tau_{hb}} \cdot \frac{V_{\text{offh}} - V}{1 - \exp\left(\frac{-(V_{\text{offh}} - V)}{V_{\text{sloh}}}\right)}$$

$$m_\infty = \frac{\alpha_m}{\alpha_m + \beta_m}$$

$$h_\infty = \frac{\alpha_h}{\alpha_h + \beta_h}$$

$$\tau_m = \frac{1}{T_{\text{adj}}(\alpha_m + \beta_m)}$$

$$\tau_h = \frac{1}{T_{\text{adj}}(\alpha_h + \beta_h)}$$

$V_{\text{offm}} = -38$  mV,  $V_{\text{offh}} = -66$  mV,  $V_{\text{slo m}} = 6.0$  mV,  $V_{\text{sloh}} = 6.0$  mV,  $\tau_{ma} = 5.49$  ms,  $\tau_{mb} = 8.06$  ms,  $\tau_{ha} = 66.67$  ms,  $\tau_{hb} = 66.67$  ms,  $\bar{g}_s = 2.04$  S/cm<sup>2</sup>,  $\bar{g}_{ad} = 0.0213$  S/cm<sup>2</sup>,  $N_m = 3$ ,  $N_h = 1$

**Persistent Na<sup>+</sup> current,  $I_{Nap}$**

$$m_\infty = \frac{1}{1 + \exp\left(\frac{V_{\text{offm}} - V}{V_{\text{slo m}}}\right)}$$

$$h_\infty = \frac{1}{1 + \exp\left(-\frac{V_{\text{offh}} - V}{V_{\text{sloh}}}\right)}$$

$$\alpha_m = -\frac{1}{\tau_{ma}} \cdot \frac{V_{\text{offma}} - V}{1 - \exp\left(\frac{(V_{\text{offma}} - V)}{V_{\text{slo ma}}}\right)}$$

$$\beta_m = \frac{1}{\tau_{mb}} \cdot \frac{V_{\text{offmb}} - V}{1 - \exp\left(\frac{-(V_{\text{offmb}} - V)}{V_{\text{slo mb}}}\right)}$$

$$\alpha_h = \frac{1}{\tau_{ha}} \cdot \frac{V_{\text{offha}} - V}{1 - \exp\left(-\frac{V_{\text{offha}} - V}{V_{\text{slo ha}}}\right)}$$

$$\beta_h = -\frac{1}{\tau_{hb}} \cdot \frac{V_{\text{offhb}} - V}{1 - \exp\left(\frac{V_{\text{offhb}} - V}{V_{\text{slo hb}}}\right)}$$

$$\tau_m = \frac{6}{T_{\text{adj}}(\alpha_m + \beta_m)}$$

$$\tau_h = \frac{1}{T_{\text{adj}}(\alpha_h + \beta_h)}$$

$V_{\text{offm}} = -52.6$  mV,  $V_{\text{slo m}} = 4.6$  mV,  $V_{\text{offma}} = -38$  mV,  $V_{\text{offmb}} = -38$  mV,  $V_{\text{slo ma}} = 6.0$  mV,  $V_{\text{slo mb}} = 6.0$  mV,  $\tau_{ma} = 5.49$  ms,  $\tau_{mb} = 8.06$  ms,  $V_{\text{offh}} = -48.8$  mV,  $V_{\text{sloh}} = 10.0$  mV,  $V_{\text{offha}} = -17$  mV,  $V_{\text{offhb}} = -64.4$  mV,  $V_{\text{slo ha}} = 4.63$  mV,  $V_{\text{slo hb}} = 2.63$  mV,  $\tau_{ha} = 347222.2$  ms,  $\tau_{hb} = 144092.2$  ms,  $\bar{g}_s = 0.00172$  S/cm<sup>2</sup>,  $N_m = 3$ ,  $N_h = 1$

**Non-specific cation current,  $I_h$**

$$\alpha_m = -\frac{1}{\tau_{ma}} \cdot \frac{V_{\text{offma}} - V}{\exp\left(-\frac{V_{\text{offma}} - V}{V_{\text{slo ma}}}\right) - 1}$$

$$\beta_m = \frac{1}{\tau_{mb}} \exp\left(-\frac{V_{\text{offmb}} - V}{V_{\text{slo mb}}}\right)$$

$$m_\infty = \frac{\alpha_m}{\alpha_m + \beta_m}$$

$$\tau_m = \frac{1}{\alpha_m + \beta_m}$$

$E = -45.0$  mV,  $V_{\text{offma}} = -154.9$  mV,  $V_{\text{slo ma}} = 11.9$  mV,  $\tau_{ma} = 155.52$  ms,  $V_{\text{offmb}} = 0.0$  mV,  $V_{\text{slo mb}} = 33.1$  mV,  $\tau_{mb} = 5.18$  ms,  $\bar{g}_s = 0.0002$  S/cm<sup>2</sup>,  $\bar{g}_{ad} = -0.00017392$  S/cm<sup>2</sup> +  $0.0004174$  S/cm<sup>2</sup> · exp(3.6161x/L<sub>max</sub>),  $\bar{g}_{bd} = 0.0002$  S/cm<sup>2</sup>,  $N_m = 1$ ,  $N_h = 0$



### Muscarinic $K^+$ current, $I_m$

$$\alpha_m = \frac{1}{\tau_{ma}} \exp\left(-\frac{V_{offma} - V}{V_{sloa}}\right)$$

$$\beta_m = \frac{1}{\tau_{mb}} \exp\left(\frac{V_{offmb} - V}{V_{slomb}}\right)$$

$$m_\infty = \frac{\alpha_m}{\alpha_m + \beta_m}$$

$$\tau_m = \frac{1}{T_{adj}(\alpha_m + \beta_m)}$$

$V_{offma} = -35$  mV,  $V_{sloa} = 10$  mV,  $\tau_{ma} = 303.03$  ms,  $V_{offmb} = -35$  mV,  $V_{slomb} = 10$  mV,  $\tau_{mb} = 303.03$  ms,  $\bar{g}_{ad} = 0.0000675$  S/cm<sup>2</sup>,  $N_m = 1$ ,  $N_h = 0$

### Slow inactivating $K^+$ current, $I_{Kp}$

$$m_\infty = \frac{1}{1 + \exp\left(\frac{V_{offm} - V}{V_{slo}}\right)}$$

$$h_\infty = \frac{1}{1 + \exp\left(-\frac{V_{offh} - V}{V_{sloh}}\right)}$$

$$\tau_m = \begin{cases} \frac{\tau_{mmin} + \tau_{mdiff1} \exp\left(-\frac{V_{offmt} - V}{V_{slo}}\right)}{T_{adj}}, & \text{if } V \leq V_{thresh} \\ \frac{\tau_{mmin} + \tau_{mdiff2} \exp\left(\frac{V_{offmt} - V}{V_{slo}}\right)}{T_{adj}}, & \text{if } V > V_{thresh} \end{cases}$$

$$\tau_h = \frac{\tau_{hmin} + (\tau_{hdiff1} - \tau_{hdiff2}(V_{offht1} - V)) \exp\left(-\left(\frac{V_{offht2} - V}{V_{sloht}}\right)^2\right)}{T_{adj}}$$

$$V_{thresh} = V_{offmt} - \frac{V_{slo}}{2} \log\left(\frac{\tau_{mdiff1}}{\tau_{mdiff2}}\right)$$

$V_{offm} = -11$  mV,  $V_{slo} = 12$  mV,  $V_{offmt} = -10$  mV,  $V_{slo} = 38.46$  mV,  $\tau_{mmin} = 1.25$  ms,  $\tau_{mdiff1} = 175.03$  ms,  $\tau_{mdiff2} = 13$  ms,  $V_{offh} = -64$  mV,  $V_{sloh} = 11$  mV,  $V_{offht1} = -65$  mV,  $V_{offht2} = -85$  mV,  $V_{sloht} = 48$  mV,  $\tau_{hmin} = 360$  ms,  $\tau_{hdiff1} = 1010$  ms,  $\tau_{hdiff2} = 24$  ms/mV,  $\bar{g}_s = 0.00223$  S/cm<sup>2</sup>,  $N_m = 2$ ,  $N_h = 1$

### Fast inactivating $K^+$ current, $I_{Kt}$

$$m_\infty = \frac{1}{1 + \exp\left(\frac{V_{offm} - V}{V_{slo}}\right)}$$

$$h_\infty = \frac{1}{1 + \exp\left(-\frac{V_{offh} - V}{V_{sloh}}\right)}$$

$$\tau_m = \frac{\tau_{mmin} + \tau_{mdiff} \exp\left(-\left(\frac{V_{offmt} - V}{V_{slo}}\right)^2\right)}{T_{adj}}$$

$$\tau_h = \frac{\tau_{hmin} + \tau_{hdiff} \exp\left(-\left(\frac{V_{offht} - V}{V_{sloht}}\right)^2\right)}{T_{adj}}$$

$V_{offm} = -10$  mV,  $V_{slo} = 19$  mV,  $V_{offh} = -76$  mV,  $V_{sloh} = 10$  mV,  $V_{offmt} = -81$  mV,  $V_{slo} = 59$  mV,  $\tau_{mmin} = 0.34$  ms,  $\tau_{mdiff} = 0.92$  ms,  $V_{offht} = -83$  mV,  $V_{sloht} = 23$  mV,  $\tau_{hmin} = 8$  ms,  $\tau_{hdiff} = 49$  ms,  $\bar{g}_s = 0.0812$  S/cm<sup>2</sup>,  $N_m = 4$ ,  $N_h = 1$

### Fast, non inactivating $K^+$ current, $I_{Kv3.1}$

$$m_\infty = \frac{1}{1 + \exp\left(\frac{V_{offm} - V}{V_{slo}}\right)}$$

$$h_\infty = \frac{1}{T_{adj} \left(1 + \exp\left(\frac{V_{offh} - V}{V_{sloh}}\right)\right)}$$

$V_{offma} = 18.7$  mV,  $V_{offmt} = -46.56$  mV,  $V_{sloa} = 9.7$  mV,  $V_{slo} = 44.14$  mV,  $\tau_{mmax} = 4.0$  ms,  $\bar{g}_s = 0.693$  S/cm<sup>2</sup>,  $\bar{g}_{ad} = 0.000261$  S/cm<sup>2</sup>,  $N_m = 1$ ,  $N_h = 0$

### High-voltage-activated $\text{Ca}^{2+}$ current, $I_{CaHVA}$

$$\alpha_m = -\frac{1}{\tau_{ma}} \cdot \frac{V_{\text{offma}} - V}{1 - \exp\left(\frac{V_{\text{offma}} - V}{V_{\text{slo ma}}}\right)}$$

$$\beta_m = \frac{1}{\tau_{mb}} \exp\left(-\frac{V_{\text{offmb}} - V}{V_{\text{slo mb}}}\right)$$

$$m_\infty = \frac{\alpha_m}{\alpha_m + \beta_m}$$

$$\tau_m = \frac{1}{\alpha_m + \beta_m}$$

$$\alpha_h = \frac{1}{\tau_{ha}} \exp\left(\frac{V_{\text{offha}} - V}{V_{\text{slo ha}}}\right)$$

$$\beta_h = -\frac{1}{\tau_{hb}} \cdot \frac{1}{1 + \exp\left(\frac{V_{\text{offhb}} - V}{V_{\text{slo hb}}}\right)}$$

$$h_\infty = \frac{\alpha_h}{\alpha_h + \beta_h}$$

$$\tau_h = \frac{1}{\alpha_h + \beta_h}$$

$V_{\text{offma}} = -27$  mV,  $V_{\text{offmb}} = -75$  mV,  $V_{\text{offha}} = -13$  mV,  $V_{\text{offhb}} = -15$  mV,  $V_{\text{slo ma}} = 3.8$  mV,  $V_{\text{slo mb}} = 17$  mV,  $V_{\text{slo ha}} = 50$  mV,  $V_{\text{slo hb}} = 28$  mV,  $\tau_{ma} = 18.18$  ms,  $\tau_{mb} = 1.06$  ms,  $\tau_{ha} = 2188.18$  ms,  $\tau_{hb} = 153.85$  ms,  $\bar{g}_s = 0.000992$  S/cm<sup>2</sup>,  $\bar{g}_{ad,hot} = 0.000555$  S/cm<sup>2</sup>,  $\bar{g}_{ad} = 0.0000555$  S/cm<sup>2</sup>,  $N_m = 2$ ,  $N_h = 1$

### Low-voltage-activated $\text{Ca}^{2+}$ current, $I_{CaLVA}$

$$m_\infty = \frac{1}{1 + \exp\left(\frac{V_{\text{offm}} - V}{V_{\text{slo m}}}\right)}$$

$$h_\infty = \frac{1}{1 + \exp\left(-\frac{V_{\text{offh}} - V}{V_{\text{slo h}}}\right)}$$

$$\tau_m = \tau_{m\text{min}} + \frac{\tau_{m\text{diff}}}{T_{\text{adj}} \left(1 + \exp\left(-\frac{V_{\text{offmt}} - V}{V_{\text{slo mt}}}\right)\right)}$$

$$\tau_h = \tau_{h\text{min}} + \frac{\tau_{h\text{diff}}}{T_{\text{adj}} \left(1 + \exp\left(-\frac{V_{\text{offht}} - V}{V_{\text{slo ht}}}\right)\right)}$$

$V_{\text{offma}} = -40.0$  mV,  $V_{\text{offmt}} = -35.0$  mV,  $V_{\text{offha}} = -90.0$  mV,  $V_{\text{offht}} = -50.0$  mV,  $V_{\text{slo ma}} = 6.0$  mV,  $V_{\text{slo mt}} = 5.0$  mV,  $V_{\text{slo ha}} = 6.4$  mV,  $V_{\text{slo ht}} = 7.0$  mV,  $\tau_{m\text{min}} = 5.0$  ms,  $\tau_{m\text{diff}} = 20.0$  ms,  $\tau_{h\text{min}} = 20.0$  ms,  $\tau_{h\text{diff}} = 50.0$  ms,  $\bar{g}_s = 0.00343$  S/cm<sup>2</sup>,  $\bar{g}_{ad,hot} = 0.0187$  S/cm<sup>2</sup>,  $\bar{g}_{ad} = 0.000187$  S/cm<sup>2</sup>,  $N_m = 2$ ,  $N_h = 1$

### Small-conductance $\text{Ca}^{2+}$ -activated $\text{K}^+$ current, $I_{SK}$

$$m_\infty = \frac{1}{1 + \left(\frac{[\text{Ca}^{2+}]_i}{c_{\text{off}}}\right)^{-c_{\text{slo}}}}$$

$c_{\text{off}} = 0.00043$  mM,  $c_{\text{slo}} = 4.8$ ,  $\bar{g}_s = 0.0441$  S/cm<sup>2</sup>,  $\bar{g}_{ad} = 0.0012$  S/cm<sup>2</sup>,  $N_m = 1$ ,  $N_h = 1$

### Leak current, $I_{leak}$

$E = -90$  mV,  $\bar{g}_s = 0.0000338$  S/cm<sup>2</sup>,  $\bar{g}_{ad} = 0.0000589$  S/cm<sup>2</sup>,  $\bar{g}_{bd} = 0.0000467$  S/cm<sup>2</sup>,  $N_m = 0$ ,  $N_h = 0$

### Intracellular $[\text{Ca}^{2+}]$ dynamics

$$\frac{d[\text{Ca}^{2+}]_i}{dt} = \frac{I_{CaHVA} + I_{CaLVA}}{2\gamma Fd} - \frac{[\text{Ca}^{2+}]_i - c_{\text{min}}}{\tau_{\text{decay}}}$$

$\gamma = 0.05$ ,  $\tau_{\text{decay}} = 80$  ms,  $d = 0.1$   $\mu\text{m}$ ,  $c_{\text{min}} = 10^{-4}$  mM

### Temperature adjustment factor

$$T_{\text{adj}} = 2.3^{\frac{34-21}{10}}$$

## Functional genomics literature review

Many of the genes that are now confirmed to be linked to SCZ, have previously been shown to play a role in regulating the activation/inactivation kinetics of certain types of cellular transmembrane currents in animal or *in vitro* studies. Typically, these studies involved transfection of ion channel-encoding DNA into cells that normally do not express the considered ion channels, and documentation on how a variant DNA changed the electrophysiological properties of the cells compared to the cells transfected with control DNA. Moreover, many studies have demonstrated the effects of certain variants of a calcium signaling toolkit gene [S1] on the dynamics of the  $\text{Ca}^{2+}$  concentration in the intracellular medium.

We searched through the literature on functional genomics for genes *CACNA1C*, *CACNB2*, *CACNA1I*, *ATP2A2*, *HCN1*, *CACNA1D*, *CACNA1S*, *SCN1A*, *SCN7A*, *SCN9A*, *KCNN3*, *KCNS3*, *KCNB1*, *KCNG2*, *KCNH7*, and *ATP2B2* to find data on how genetic variations change the ion channel behavior or intracellular  $\text{Ca}^{2+}$  dynamics. Due to shortness of data reported for a single animal and cell type, we included studies performed in various animal species and across different tissues. We concentrated on studies that fulfilled the following conditions:

- The study applied a genetic variant of one of the genes of interest and the gene is likely to be expressed in L5PCs.
- The properties of the cell expressing the gene variant were studied using electrophysiology or  $\text{Ca}^{2+}$  imaging.
- The deviation between the variant cell property and the control cell property could be implemented in the applied neuron model [S2] as a change of a model parameter value.
- The observed effect of the gene variant was not solely on the expression or ion channel density level.

The last condition, which ruled out studies where the effect was only shown on channel density, was set due to the multitude of pathways that may contribute to such an effect [S3]. By contrast, the effects on channel kinetics (activation and inactivation threshold potentials, sensitivity to membrane potential, and opening/closing time constants) were expected to be more straightforwardly dependent on the way these channels are genetically coded. However, data on differences in ion channel expression bear an important aspect of the total ionic behavior as well, and should therefore be introduced in the future, although compensatory mechanisms may contribute to cancel the effects of changes in expression *in vivo* (cf. [S4]).

Table 1 shows all studies that were found to obey the above conditions. An expansion of this table is given in Table S1, added with details about the effects of each variant and the underlying experimental data. The six first genes of Table 1 belong to the calcium signaling toolkit. The genes *CACNA1C*, *CACNB2*, and *CACNA1D*, encode  $\alpha$  or  $\beta$  subunits of HVA  $\text{Ca}^{2+}$  channels, and *CACNA1I* gene encodes an  $\alpha$  subunit of an LVA  $\text{Ca}^{2+}$  channel. Genes *ATP2A2* and *ATP2B2* encode intracellular  $\text{Ca}^{2+}$  transporters, namely sarco/endoplasmic reticulum  $\text{Ca}^{2+}$  ATPase (SERCA) and plasma membrane  $\text{Ca}^{2+}$  ATPase (PMCA). The rest of the listed genes encode ion channels of other ionic species. *SCN1A* and *SCN9A* encode  $\alpha$  subunits of  $\text{Na}^+$  channels, which we considered to contribute to the currents  $I_{Nat}$  and  $I_{Nap}$  in the neuron model. *KCNB1* encodes a subunit that contributes to the slow, delayed rectifier  $\text{K}^+$  current in L5PCs [S5, S6], which is denoted by  $I_{Kp}$  in the neuron model. *KCNS3* encodes an electrically silent subunit, which yet together with the subunit encoded by *KCNB1* forms slowly inactivating  $\text{K}^+$  channels [S5, S7]: these channels contribute to the current  $I_{Kp}$  as well. *KCNN3* encodes a subunit for a  $\text{Ca}^{2+}$ -activated small-conductance  $\text{K}^+$  channel (contributing to  $I_{SK}$ ), and *HCN1* encodes a subunit for a non-specific ion channel (contributing to  $I_h$ ). Not all of these genes have been shown to be expressed in thick-tufted L5PCs in specific, however, we confirmed in Allen Brain Atlas (mouse) and Human Protein Atlas that they all show expression in the cortex. Certain studies on *CACNA1S* fulfilled all other above conditions, but the gene is not expressed anywhere in the brain, and therefore we disregarded them.

Some of the studies cited in Table 1 considered several variant types, and in these cases, the range of possible effects on model parameters is considered (see Table S1). If the range spanned both increasing and decreasing effects, the analyses were carried out for both end points of the range, otherwise only the maximal deviation from the control value was considered. Also, in case one of the end points of the range was very close to the control value, namely, at a distance less than 1 mV or less than 10% of the distance between control value and the other end point, only the endpoint with the larger deviation was considered.

The applied model of an L5PC is relatively abundant in biological detail, yet it groups together many different types of currents under one model current. This represents a hindrance to carrying out detailed computational studies on the contribution of different genes to neuron firing behavior. As for our study, for this reason we could not make a distinction between the contributions of L-, N-, P-, and Q-type channels (HVA  $\text{Ca}^{2+}$  current channels) to the activation of the SK current, which have been experimentally studied in e.g. [S8]. Taking into account this particular distinction would be an important extension to our modeling framework, as many of the SCZ-related  $\text{Ca}^{2+}$  channel-encoding genes specifically encode L-type channel subunits (*CACNA1C*, *CACNA1D*, *CACNA1S*, *CACNB2*). Nevertheless, currently there are no L5PC models that would allow this.

## Scaling of gene variants

Due to the polygenic nature of SCZ, it has been proposed that none of the SCZ-related SNPs can alone cause the disorder, and that the disease may only be induced when sufficiently many of them are represented. This paradigm was adopted into the computational study at hand as follows. We first identified the parameter changes in the L5PC model [S2] that corresponded to the effects of a certain genetic variant. We then ran simulations on the neuron model, exploring the effects of one variant separately on the neuron's response to selected stimuli. If the variant altered the neural response dramatically, the genetic effect was scaled down (i.e. parameters were brought closer to the control values), so that there were no large

discrepancies between the control neuron and the mutant with the downscaled variant. The criteria for the downscaling were that no variant should alone change the number of action potentials to chosen stimuli or radically change the steady-state firing behavior of the neuron (control neuron referring to the model neuron exactly as described in [S2]). This approach was used in order to simulate the SCZ-related SNP effects, many of which are known to be subtle (cf. [S9]) in contrast to the large phenotypic effects caused by the variants of Table 1.

To scale down the effects of the variants of Table S1, the following procedure was applied. Firstly, a “standard spiking behavior” was defined as a firing behavior that fulfils the following five conditions:

- (I) Exactly 4 spikes should be induced as a response to somatic square-current injection of 0.696 nA x 150 ms,
- (II) Exactly 1 spike should be induced as a response to a distal (620  $\mu\text{m}$  from soma) alpha-shaped synaptic conductance (time constant 5 ms, max. amplitude 0.0612  $\mu\text{S}$ ),
- (III) Exactly 2 spikes should be induced as a response to a combined stimulus of somatic square-current injection (1.137 nA x 10 ms) and distal synaptic conductance (time constant 5 ms, max. amplitude 0.100  $\mu\text{S}$ , applied 5ms after the somatic pulse),
- (IV) The integrated difference between the f-I curves of the considered neuron and the control neuron should not be more than 10% of the integral of the control neuron f-I curve, and
- (V) The membrane potential limit cycle should not be too different from the control neuron limit cycle ( $d_{cc}(lc_1, lc_2) \leq 600$ , see the section below for details).

The above-mentioned amplitudes 0.696 nA, 0.0612  $\mu\text{S}$ , and 1.137 nA were chosen such that the control neuron most stably produces the named numbers of spikes with the default parameters — most stably in the sense that an equal change in current amplitude on logarithmic scale is required in order to produce one spike more or to produce one spike less. The conditions I–III restrict the magnitudes of short-time responses of the neuron, while the conditions IV–V concern continuous, steady-state firing. Secondly, the spiking behavior of cells expressing the genetic variations listed in Table 1 under the same stimuli is simulated. In case one or more of the conditions I–V are violated, the effect is scaled down, all parameters in proportion, to a fraction  $c < 1$  of the original effect where the violation is for the first time observed. These threshold effect factors  $c$  are listed in Table 2 for each variant together with the corresponding parameter changes, and the six variants that were used in Figures 2–6 are highlighted. As we do not know how small a parameter change effect should be to correspond to a small SNP effect, we consider variants with different scalings where the threshold effect factor  $c$  is multiplied with another factor  $\epsilon < 1$ . In this work, we consider the scaling factor values  $\epsilon = \frac{1}{2}$  and  $\frac{1}{4}$ , and we also display the effects of the corresponding opposite variants  $\epsilon = -\frac{1}{2}$  and  $-\frac{1}{4}$ .

For those unscaled variants that did not violate the conditions I–V, we sought for the threshold effect up to twice the original effect, i.e.  $c < 2$ . If the variant still obeyed conditions I–V, we considered the original variant the  $\epsilon = \frac{1}{2}$  variant and applied other scalings with respect to this choice.

The model parameters affected by the variants include quantities of various roles and dimensions (mV, mM, ms, etc.), which calls for a careful consideration how to scale them properly. We chose to perform this such that those parameters that may receive both negative and positive values were scaled linearly, while the parameters that receive only positive values were scaled on the logarithmic scale. In practice, this means that the differences in offset and reverse potentials ( $V_{\text{offm}*}$ ,  $V_{\text{offh}*}$ ,  $E_{\text{Ih}}$ ) between control and variant neuron were expressed as an additive term ( $\pm x$  mV), and this term  $x$  was multiplied by a factor  $c \in [0, 1]$  in the downscaling procedure. By contrast, the differences in all the other model parameters ( $V_{\text{offc}*}$ ,  $V_{\text{slo}*}$ ,  $\tau_*$ ,  $c_*$ ,  $\gamma_*$ ) between control and variant neuron were expressed as a multiplication ( $\times x$ ), where the downscaling caused this coefficient  $x$  to be exponentiated by the same factor  $c$ . This procedure permits a continuum of parameter changes in the range  $c \in [0, 1]$  that is directly applicable to amplified ( $c > 1$ ) parameter changes as well. As an example, consider the mid-point of activation of the slow inactivating  $\text{K}^+$  channel,  $V_{\text{offm},\text{Kp}} = -11$  mV. One of the variants of KCNB1 gene (fifth in Table 2) shifted this value by +14 mV, which gives the new value  $V'_{\text{offm},\text{Kp}} = 3$  mV. In such a case, it is not possible scale the parameter logarithmically, as the factor  $x = V'_{\text{offm},\text{Kp}}/V_{\text{offm},\text{Kp}}$  to be exponentiated is negative. As a contrary example, the same variant changes the time constants of activation,  $\tau_{\text{m}*,\text{Kp}}$ , by  $-61\%$ . In principle, this effect could be scaled both logarithmically and linearly in the range  $c \in [0, 1]$ . However, if the unscaled variant does not cause a violation of conditions I–V, we would study the effects of an “upscaled” variant all the way until  $c = 2$ . This would not be possible using linear scaling, as we would have to decrease the time constants of activation by  $122\%$ , leading to negative time constants.

## A distance metric for membrane potential limit cycles

A membrane potential limit cycle can be described as a 1-dimensional manifold in the space  $\mathcal{LC} = \mathcal{V} \times d\mathcal{V}$ , where  $\mathcal{V}$  is the space of possible values for membrane potentials and  $d\mathcal{V}$  is the space of possible values for time derivatives of membrane potential. Due to the difference in units for  $x$  and  $y$  axis, there is no obvious metric for this space, but such can easily be constructed. We define a bijection  $f : \mathcal{LC} \rightarrow \mathbb{R}^2$  as

$$f(V, dV) = \left( \frac{V}{1.0 \text{ mV}}, \frac{dV}{7.026 \text{ mV/ms}} \right),$$

where the constant 7.026 was chosen such that the control neuron limit cycle spans an equal range on  $x$  and  $y$  axes when the soma is given a DC of amplitude 1.0 nA. Now, a distance metric in  $d : \mathcal{LC} \times \mathcal{LC}$  can be defined as

$$d(x, y) = \|f(x) - f(y)\|_2,$$

where  $\|\cdot\|_2$  is a Euclidean norm. Furthermore, the distance of a point  $x \in \mathcal{LC}$  from a limit cycle  $lc \subset \mathcal{LC}$  can be defined as

$$d_c(x, lc) = \min_{y \in lc} \|f(x) - f(y)\|.$$

To evaluate the difference between two limit cycles  $lc_1, lc_2 \in \mathcal{LC}$ , we define

$$d_{cc}(lc_1, lc_2) = \frac{1}{2} \int_{lc_1} d_c(x, lc_2) dx + \frac{1}{2} \int_{lc_2} d_c(x, lc_1) dx.$$

Using the average of the two integrals makes sure that no part of either limit cycle is ignored: If only integral over points of  $lc_1$  was used, the limit cycle  $lc_2$  could have any “extra” part, for example an unusually long and slow hyperpolarization period or minor suboscillations, that might largely be disregarded in the integration as there are always some other points in  $lc_2$  that lie nearer to  $lc_1$ .

Table S1: Table of genetic variants and their maximal effects on our neuron model parameters. The first column of the table shows the gene whose variant is studied. The second column shows the model parameters that are affected by the variant, as the third column shows the size of the effect. The fourth column gives the PubMed index of the article, where the effects of the variant are measured. The fifth column names the type of variant used, while the sixth and seventh columns show the cell type in which the effects are measured and the animals species used in the study. The final column may give extra information. The variants are listed in the order of genes that they affect. Asterisks represent an identical change to a set of variables as follows (applicable to those variables that exist in the considered ion channel type): *offm\** refers to variables  $V_{offm}$ ,  $V_{offma}$  and  $V_{offmb}$ ; *offh\** refers to variables  $V_{offh}$ ,  $V_{offha}$  and  $V_{offhb}$ ; *slo\** refers to variables  $V_{sloa}$  and  $V_{slob}$ ; *sloh\** refers to variables  $V_{sloha}$  and  $V_{sloh}$ ; *taum\** refers to variables  $\tau_{ma}$ ,  $\tau_{mb}$ ,  $\tau_{min}$ ,  $\tau_{diff}$ ,  $\tau_{diff1}$  and  $\tau_{diff2}$ ; *tauh\** refers to variables  $\tau_{ha}$ ,  $\tau_{hb}$ ,  $\tau_{hmin}$ ,  $\tau_{hdiff}$ ,  $\tau_{hmean}$ ,  $\tau_{hdiff1}$  and  $\tau_{hdiff2}$ .

Gene	Model parameter	Effect	Paper	Type of variant	Cell type	Animal	Notes
CACNA1C	<i>offm*</i> _CaHVA <i>offh*</i> _CaHVA	-25.9..-1.4 mV -27.0..-3.8 mV	pubmed/19265197	L429T, L434T, S435T, S435A S435P	TSA201	human	-These represent variant of the IS6 segment
CACNA1C	<i>offm*</i> _CaHVA <i>offh*</i> _CaHVA	-37.3..-9.7 mV -30.0..-11.8 mV	pubmed/19265197	L779T, I781T, I781P	TSA201	human	-These are variants of IIS6 segment. Double (IIS6+IS6) mutant seems to have additive effect
CACNB2	<i>offh*</i> _CaHVA <i>sloh*</i> _CaHVA	-5.2 mV -31%	pubmed/19358333	T11I-mutant	TSA201	human	-Small changes shown in <i>offma</i> , <i>offmb</i> and <i>tau</i> ignored
CACNB2	<i>taum*</i> _CaHVA	+70%	pubmed/7723731	A1B2 vs A1 alone	HEK293	human/mouse	
CACNB2	<i>offm*</i> _CaHVA <i>offh*</i> _CaHVA <i>taum*</i> _CaHVA <i>tauh*</i> _CaHVA	-4.9..+4.9mV -5.1..+5.1mV -40%..+68% -40%..+66%	pubmed/19723630	N1 vs N3 vs N4 vs N5	HEK293	human/mouse	-Changes to voltage-dependence of <i>taus</i> ignored.
CACNA1D	<i>offm*</i> _CaHVA <i>slo*</i> _CaHVA <i>offh*</i> _CaHVA <i>sloh*</i> _CaHVA <i>tauh*</i> _CaHVA	-10.9..-8.5mV -27..-13% -3.0..+3.5mV -12..-19% +25%	pubmed/21998309 pubmed/21998310	42A splices transfected (Alternative splicing at C-terminus)	TSA201/HEK293	human	-The variants are expressed in human and mouse brains; hence, the effect of genetic variances could be of opposite sign with respect to control
CACNA1D	<i>offm*</i> _CaHVA <i>slo*</i> _CaHVA <i>offh*</i> _CaHVA <i>sloh*</i> _CaHVA <i>tauh*</i> _CaHVA	-10.6..+3.4mV -20..+12% -5.3..+1.2mV -34..-8% -28%	pubmed/21998309 pubmed/21998310	43S splices transfected (Alternative splicing at C-terminus)	TSA201/HEK293	human	-The variants are expressed in human and mouse brains; hence, the effect of genetic variances could be of opposite sign with respect to control
CACNA1D	<i>offm*</i> _CaHVA <i>slo*</i> _CaHVA <i>tauh*</i> _CaHVA	+3.5..+6.6mV -25..+19% -50..+12%	pubmed/20951705 pubmed/21054386	CaV1.3 (-/-) vs control	AV node cells/ chromaffin cells	mouse	-Some time constants compared between single <i>tau</i> fits (as double <i>tau</i> fits not always well fitted)
CACNA1I	<i>offma*_CaLVA</i> <i>offha*_CaLVA</i> <i>taum*_CaLVA</i> <i>tauh*_CaLVA</i>	-0.2..+1.3mV -0.5..+1.6mV -13..+45% -20..+8%	pubmed/15254077	Alternative splicing of exons 9 and 33	HEK293	human	-Maximum of effects at -40 or 0 mV on kinetics considered -Changes in slope minuscule
ATP2A2	<i>gamma*_CaDyn</i>	-30..-40%	pubmed/10970890	Heter. null mutation	myocytes	mouse	-Compensating mechanisms exist that prevent larger effects
ATP2B2	<i>decay*_CaDyn</i>	+15..+113%	pubmed/22789621	Heter. knockout	Purkinje cells	mouse	-Compensatory mechanisms exist that prevent larger effects
ATP2B2	<i>decay*_CaDyn</i> <i>minCa1*_CaDyn</i>	+32..+50% +40%	pubmed/21232211	Homozyg. knockout	Purkinje cells	mouse	
ATP2B2	<i>decay*_CaDyn</i>	+53..+345%	pubmed/17234811	G283S-,G293S-mutant	CHO cells	human/mouse	-+53% for G293S, +345% for G283S
SCN1A	<i>offm*_Nat</i> <i>offh*_Nat</i> <i>slo*_Nat</i> <i>sloh*_Nat</i>	-0.3mV +5.0mV +15% +23%	pubmed/18632931	FHM mutation Q1489K	Neocortex (cultured)	human/rat	-Slow inactivation could not be studied in detail in neurons
SCN1A	<i>offm*_Nat</i> <i>offh*_Nat</i> <i>slo*_Nat</i> <i>sloh*_Nat</i>	+2.8mV +9.6mV -1.6% +4.2%	pubmed/17397047	FHM mutation L1649Q	TSA201	human	-Electrophysiology done with the corresponding mutation L1636Q in the homologous SCN5A gene due to instabilities in recomb. bacteria
SCN9A	<i>offh*_Nap</i>	+6.8mV	pubmed/22136189	I228M NaV1.7 variant	HEK293	human	-Differences in activation and fast inactivation not significant
SCN9A	<i>offh*_Nap</i> <i>sloh*_Nap</i> <i>offm*_Nat</i> <i>offh*_Nat</i> <i>sloh*_Nat</i>	+3.5mV -45% -7.1mV +17.0mV -31%	pubmed/18945915	A1632E NaV1.7 mutation	HEK293	human	-Slow inactivation interpreted as inactivation of persistent (Nap) current and fast inactivation as inactivation of transient (Nat) current
SCN9A	<i>offm*_Nat</i> <i>offh*_Nat</i>	-9.1mV +3.1mV	pubmed/16392115	L858F NaV1.7 mutation	HEK293	human	-Activation and inact. curves closer to Nat than Nap currents
SCN9A	<i>offm*_Nat</i> <i>offh*_Nat</i>	-7.6mV +4.3mV	pubmed/15958509	F1449V NaV1.7 mutation	HEK293	human	-Activation and inact. curves closer to Nat than Nap currents
KCNB3	<i>taum*_Kp</i> <i>tauh*_Kp</i> <i>sloh*_Kp</i>	0..+100% +50..+150% -50%	pubmed/10484328	hKv2.1-(G4S)3-hKv9 fusion inserted (or hKv9 inserted explicitly)	HEK293	human	-Fits not carried out in the paper, approximate values used.
KCNB1	<i>offm*_Kp</i> <i>offh*_Kp</i> <i>slo*_Kp</i> <i>sloh*_Kp</i> <i>taum*_Kp</i> <i>tauh*_Kp</i>	+5mV +3mV +11% -14% -50% -47%	pubmed/21455829	T203K mutant	HEK293	human/mouse	-Double mutations studied as well, but they are not included here
KCNB1	<i>offm*_Kp</i> <i>offh*_Kp</i> <i>slo*_Kp</i> <i>sloh*_Kp</i> <i>taum*_Kp</i>	+1mV -6mV +22% +0% -11%	pubmed/21455829	T203D mutant	HEK293	human/mouse	

	tauh*_Kp	-13%					
KCNB1	offm_Kp offh_Kp sloM_Kp sloh_Kp taum*_Kp tauh*_Kp	+6mV -8mV +33% +0% -50% -13%	pubmed/21455829	S347K mutant	HEK293	human/mouse	
KCNB1	offm_Kp offh_Kp sloM_Kp sloh_Kp taum*_Kp tauh*_Kp	-28mV -27mV +11% -29% +13% +127%	pubmed/21455829	S347D mutant	HEK293	human/mouse	
KCNB1	offm_Kp offh_Kp sloM_Kp sloh_Kp taum*_Kp tauh*_Kp	+14mV -21mV +100% +0% -61% +20%	pubmed/21455829	T203W mutant	HEK293	human/mouse	
KCNB1	offm_Kp offh_Kp sloM_Kp sloh_Kp taum*_Kp tauh*_Kp	-13mV -13mV +33% -29% -5% +413%	pubmed/21455829	S347W mutant	HEK293	human/mouse	
KCNN3	offc_SK sloc_SK	-14% +24%	pubmed/14978258	hSK3_ex4 isoform	TSA	human	-Activation curve constructed a bit differently from Hay model
HCN1	offm*_Ih sloM*_Ih	-2.1..-26.5mV -12..-36%	pubmed/17185333	D135W, D135H, D135N mutants	HEK293	human/mouse	-Other mutations studied as well, but they change the Ih current too dramatically

## Supplemental results

Here, we extended the analyses carried out for the variants of Figures 2–6 by considering additional variants. Figures S1 and S2 show a compilation of statistics related to Figures 3–6 for all variants of Table 2: Figure S1 illustrates the range of steady-state  $\text{Ca}^{2+}$  concentration oscillation, while Figure S2 shows the mean firing rate across the DC amplitudes used in the f-I curves, the temporal sensitivities of the  $\text{Ca}^{2+}$  spike during up and down states, and the time window for an efficient suppression of a second apical stimulus. In Figure S1, the results are additionally plotted for the unscaled variants for reference, while in Figure S2, only unscaled variants are considered. The results of Figure S2 for the positively scaled ( $\epsilon = \frac{1}{2}$ ) variant are also summarized in Table S2. Except for genes *KCNS3* and *KCNB1*, variants of all genes showed a notable impact on some of these statistics.

Changes in intracellular  $[\text{Ca}^{2+}]$  may be functionally relevant for many neural processes. Intracellular  $[\text{Ca}^{2+}]$  plays an important role in the activation of various second messenger cascades, which control a variety of cellular processes [S4, S10–S13], but these aspects are out of the scope of the current work. A more immediate effect of intracellular  $[\text{Ca}^{2+}]$  is the activation of  $\text{Ca}^{2+}$ -dependent  $\text{K}^+$  -currents, such as the small-conductance  $\text{K}^+$  current ( $I_{SK}$ ). This current was included in the L5PC-model, and it is affected by the *KCNN* gene family. In Figure 2, the effects of the *KCNN3* variant were undetectable. This was because  $I_{SK}$  currents are large only when both intracellular  $[\text{Ca}^{2+}]$  and the membrane potential are elevated — although the currents only need high  $[\text{Ca}^{2+}]$  to be activated, they can be large only when the membrane potential is far enough from the  $\text{K}^+$  reversal potential, which is relatively near to the membrane resting potential. The effects of the *KCNN3* variant could be detected when a more enduring stimulus than a brief somatic pulse was applied, as done in Figures 3–6: these effects can also be observed in Figures S1 and S2.

Most of the variants that gave positive shift in  $[\text{Ca}^{2+}]$  (Figure S1), also resulted in reduced firing rates (Figure 3). There was a correlation coefficient of -0.70 between the maximal  $[\text{Ca}^{2+}]$  value in the limit cycle and the integral of the measured f-I curve. An exception to this trend was the *KCNN3* variant, where the threshold  $[\text{Ca}^{2+}]$  was lower (in the positively scaled variants) than in the control neuron, see Table 2. When stimulated with the DC of amplitude 1.2 nA (Figure 4), this lower threshold caused the SK current to be upheld for a longer time after the spike than in the control neuron. This caused a delay in the timing of the next spike, allowing the  $[\text{Ca}^{2+}]$  to drop to a lower value before the next spike, and hence the oscillation of the  $[\text{Ca}^{2+}]$  remained at an overall lower level than in the control neuron (data not shown).

## Combinations of variants may cause large alterations of neuron excitability

The effects of the variants on neuron excitability, as explored in Figures 2–6, were relatively small when the variants were studied in isolation (this was also the intention behind the downscaling process). However, combinations of variants of different genes may have additive effects on the neuron excitability. We investigated the effect that combinations of several of the variants could have. Figure S3 shows a selected example of how a combination of variants altered the neuron firing properties considered in Figures 2–6. Although this version of the model neuron consists of downscaled variants, the properties of neuron excitability were remarkably modified.

In Figure S3, the selection was based on the property of inhibiting the second apical stimulus as shown in Figure 6: We combined such downscaled variants that had a lower threshold curve than the control neuron, i.e., variants that made it easier for the second apical stimulus to induce a spike, however picking maximum one variant per gene. See Table 2 for this selection. Large impacts of the combination of variants could be seen in both  $\text{Ca}^{2+}$  responses (Figure S3A-B, S3D), temporal profiles of  $\text{Ca}^{2+}$  spike generation (Figure S3E), and naturally the inhibition of a second stimulus (Figure S3F). The change in gain (Figure S3E) was nevertheless minor: Although all variants of the combination caused an increase in gain when in isolation (except for the *CACNA1I* variant which had a minuscule effect and *KCNN3* variant which had an ambiguous effect), these increases in gain were in most cases caused by an overall decrease in  $\text{Ca}^{2+}$  currents. These changes were compensated for by a decrease of threshold  $[\text{Ca}^{2+}]$  of the SK current that is characteristic of the *KCNN3* variant, and hence the resulting f-I curve was relatively close to that of the control neuron.

The effect of the combination of variants on the  $\text{Ca}^{2+}$  spike generation in Figure S3E is notable. The sensitivity of the  $\text{Ca}^{2+}$  spike magnitude to the ISI could serve as a coincidence detection mechanism of synaptic inputs projected to different parts of the L5PC and thus form an important element in cortical information processing. A widening of the region of ISIs that produce a large  $\text{Ca}^{2+}$  spike could weaken the coincidence detection ability of the neuron [S14], while an extensive narrowing of the curve would limit the regime for  $[\text{Ca}^{2+}]$  spike generation [S15] and hence contribute with a lesser total excitability. In the up-state protocol, the combination of  $\epsilon = \frac{1}{4}$  variants only produce minor  $\text{Ca}^{2+}$  spikes, and their temporal ISI window is narrowed down, while the combination of  $\epsilon = \frac{1}{2}$  variants does not produce a  $\text{Ca}^{2+}$  spike at all with the considered stimuli.

Due to lack of data on the interplay between different variants of a single gene, we only implemented a maximum of one variant per gene when we simulated combinations of variants. There is, however, evidence that SNPs or other variants located in different parts of the same gene may have additive effects on the ion channel kinetics, as shown in the case of mutations in different parts of the *CACNA1C* gene [S16]. Hence, given detailed information on such effects in other genes as well, the predictive power of our method could still be improved by allowing more diverse combinations of the same set of variants.

## Robustness of the analyses

To study the robustness of our findings, we performed similar analyses in a neuron model using an alternative set of fitted model parameters. We implemented the alternative neuron model, “Model 1”, as given in the first column of Table S1 in [S2].



The scaling of the variants was redone in this neuron model, and the variant neuron behaviour was quantified in a similar manner as done for the primary fit. Figure S4 shows the compilation of results obtained from the alternative model. The results are qualitatively similar for the majority of the variants. The only observable exceptions are the 12th variant in the third group of *CACNB2* variants and the second variant in the second group of *CACNA1D* variants, which caused a large depression of the  $\text{Ca}^{2+}$  spike in the up-state protocol of the primary neuron model, shown as a missing bar in Figure S2C. By contrast, the dendritic membrane potential response in the same variants of the alternative neuron model did exceed the set threshold, leading to an observed (but narrowed-down) temporal window in Figure S4C.

We further analyzed the robustness of our findings using the primary neuron model fit but in an alternative neuron morphology. We applied and downscaled our variants using the cell #2 morphology of [S2], and performed the same analyses as done with the primary neuron morphology, cell #1. The firing rates were in general smaller in cell #2: A somatic DC of amplitude 1.2 nA caused the control neuron to fire with a frequency of 15.4 Hz, whereas the corresponding rate in cell #1 was 16.9 Hz. The up- and down-state protocols did not produce responses directly comparable those of cell #1, and hence, we omitted these analyses in cell #2. By contrast, the property of inhibiting a second apical stimulus was preserved in cell #2, although in a slightly different regime. In cell #2, a nearly doubled maximal conductance w.r.t. that in cell #1 was required to make the neuron spike when the synaptic inputs were uniformly distributed along the apical dendrite ( $g_{th} = 5.0 \mu\text{S}$  vs.  $2.8 \mu\text{S}$  in cell #1). Accordingly, the ratio  $c_g$  between the threshold conductance for eliciting a second spike and that for eliciting the first spike ( $g_{th}$ ) was lower: In the control case of cell #2, the factor  $c_g$  varied from 0.44 to 1.91, while the corresponding range in cell #1 was from 0.51 to 5.13. To compensate for this effect, we analyzed the PPI temporal window in terms of a lower threshold factor, namely, we measured the first and last ISI for which  $c_g$  exceeded the value 1.5 (3.0 in cell #1).

The compilation of results obtained from simulations with cell #2 are shown in Figure S5. The amplitudes of variant effects are different than in cell #1 (see Figure S2), but the direction of the variant effects are the same as in cell #1.

## References

- S1. MJ Berridge, P Lipp, and MD Bootman. “The versatility and universality of calcium signalling”. In: *Nature Rev Mol Cell Biol* 1.1 (2000), pp. 11–21.
- S2. E Hay, S Hill, F Schürmann, H Markram, and I Segev. “Models of neocortical layer 5b pyramidal cells capturing a wide range of dendritic and perisomatic active properties”. In: *PLoS Comput Biol* 7 (2011), e1002107.
- S3. B Rosati and D McKinnon. “Regulation of ion channel expression”. In: *Circ Res* 94.7 (2004), pp. 874–883.
- S4. T O’Leary, AH Williams, A Franci, and E Marder. “Cell types, network homeostasis, and pathological compensation from a biologically plausible ion channel expression model”. In: *Neuron* 82.4 (2014), pp. 809–821.
- S5. D Guan, T Tkatch, D Surmeier, W Armstrong, and R Foehring. “Kv2 subunits underlie slowly inactivating potassium current in rat neocortical pyramidal neurons”. In: *J Physiol* 581.3 (2007), pp. 941–960.
- S6. A Korngreen and B Sakmann. “Voltage-gated K<sup>+</sup> channels in layer 5 neocortical pyramidal neurones from young rats: subtypes and gradients”. In: *J Physiol* 525.3 (2000), pp. 621–639.
- S7. AR Shepard and JL Rae. “Electrically silent potassium channel subunits from human lens epithelium”. In: *Am J Physiol-Cell Ph* 277.3 (1999), pp. C412–C424.
- S8. JC Pineda, RS Waters, and RC Foehring. “Specificity in the interaction of HVA Ca<sup>2+</sup> channel types with Ca<sup>2+</sup>-dependent AHPs and firing behavior in neocortical pyramidal neurons”. In: *J Neurophysiol* 79.5 (1998), pp. 2522–2534.
- S9. SH Lee, TR DeCandia, S Ripke, J Yang, PF Sullivan, ME Goddard, MC Keller, et al. “Estimating the proportion of variation in susceptibility to schizophrenia captured by common SNPs”. In: *Nat Gen* 44.3 (2012), pp. 247–250.
- S10. WA Catterall. “Structure and function of neuronal Ca<sup>2+</sup> channels and their role in neurotransmitter release”. In: *Cell Calcium* 24.5 (1998), pp. 307–323.
- S11. E Perez-Reyes. “Molecular physiology of low-voltage-activated t-type calcium channels”. In: *Physiol Rev* 83.1 (2003), pp. 117–161.
- S12. HC Pape, T Munsch, and T Budde. “Novel vistas of calcium-mediated signalling in the thalamus”. In: *Pflugers Arch* 448.2 (2004), pp. 131–138.
- S13. J Lee, K Song, K Lee, J Hong, H Lee, S Chae, E Cheong, et al. “Sleep spindles are generated in the absence of T-type calcium channel-mediated low-threshold burst firing of thalamocortical neurons”. In: *Proc Natl Acad Sci* 110.50 (2013), pp. 20266–20271.
- S14. E Calixto, EJ Galván, JP Card, and G Barrionuevo. “Coincidence detection of convergent perforant path and mossy fibre inputs by CA3 interneurons”. In: *J Physiol* 586.11 (2008), pp. 2695–2712.
- S15. D Ledergerber and ME Larkum. “The time window for generation of dendritic spikes by coincidence of action potentials and EPSPs is layer specific in somatosensory cortex”. In: *PLoS ONE* 7.3 (2012), e33146.
- S16. M Kudrnac, S Beyl, A Hohaus, A Stary, T Peterbauer, E Timin, and S Hering. “Coupled and independent contributions of residues in IS6 and IIS6 to activation gating of CaV1.2”. In: *J Biol Chem* 284.18 (2009), pp. 12276–12284.

- S17. JM Cordeiro, M Marieb, R Pfeiffer, K Calloe, E Burashnikov, and C Antzelevitch. “Accelerated inactivation of the L-type calcium current due to a mutation in CACNB2b underlies Brugada syndrome”. In: *J Mol Cell Cardiol* 46.5 (2009), pp. 695–703.
- S18. E Massa, KM Kelly, DI Yule, RL MacDonald, and MD Uhler. “Comparison of fura-2 imaging and electrophysiological analysis of murine calcium channel alpha 1 subunits coexpressed with novel beta 2 subunit isoforms”. In: *Mol Pharmacol* 47.4 (1995), pp. 707–716.
- S19. S Link, M Meissner, B Held, A Beck, P Weissgerber, M Freichel, and V Flockerzi. “Diversity and developmental expression of L-type calcium channel  $\beta 2$  proteins and their influence on calcium current in murine heart”. In: *J Biol Chem* 284.44 (2009), pp. 30129–30137.
- S20. BZ Tan, F Jiang, MY Tan, D Yu, H Huang, Y Shen, and TW Soong. “Functional characterization of alternative splicing in the C terminus of L-type CaV1.3 channels”. In: *J Biol Chem* 286.49 (2011), pp. 42725–42735.
- S21. G Bock, M Gebhart, A Scharinger, W Jangsangthong, P Busquet, C Poggiani, S Sartori, et al. “Functional properties of a newly identified C-terminal splice variant of Cav1.3 L-type Ca<sup>2+</sup> channels”. In: *J Biol Chem* 286.49 (2011), pp. 42736–42748.
- S22. Q Zhang, V Timofeyev, H Qiu, L Lu, N Li, A Singapuri, CL Torado, et al. “Expression and roles of Cav1.3 ( $\alpha 1D$ ) L-type Ca<sup>2+</sup> channel in atrioventricular node automaticity”. In: *J Mol Cell Cardiol* 50.1 (2011), pp. 194–202.
- S23. A Pérez-Alvarez, A Hernández-Vivanco, JC Caba-González, and A Albillos. “Different roles attributed to Cav1 channel subtypes in spontaneous action potential firing and fine tuning of exocytosis in mouse chromaffin cells”. In: *J Neurochem* 116.1 (2011), pp. 105–121.
- S24. J Murbartián, JM Arias, and E Perez-Reyes. “Functional impact of alternative splicing of human T-type Cav3.3 calcium channels”. In: *J Neurophysiol* 92.6 (2004), pp. 3399–3407.
- S25. Y Ji, MJ Lalli, GJ Babu, Y Xu, DL Kirkpatrick, LH Liu, N Chiamvimonvat, et al. “Disruption of a single copy of the SERCA2 gene results in altered Ca<sup>2+</sup> homeostasis and cardiomyocyte function”. In: *J Biol Chem* 275.48 (2000), pp. 38073–38080.
- S26. AK Fakira, LD Gaspers, AP Thomas, H Li, MR Jain, and S Elkabes. “Purkinje cell dysfunction and delayed death in plasma membrane calcium ATPase 2-heterozygous mice”. In: *Mol Cell Neurosci* 51.1 (2012), pp. 22–31.
- S27. RM Empson, W Akemann, and T Knöpfel. “The role of the calcium transporter protein plasma membrane calcium ATPase PMCA2 in cerebellar Purkinje neuron function”. In: *Funct Neurol* 25.3 (2010), p. 153.
- S28. R Ficarella, F Di Leva, M Bortolozzi, S Ortolano, F Donaudy, M Petrillo, S Melchionda, et al. “A functional study of plasma-membrane calcium-pump isoform 2 mutants causing digenic deafness”. In: *Proc Natl Acad Sci* 104.5 (2007), pp. 1516–1521.
- S29. S Cestèle, P Scalmani, R Rusconi, B Terragni, S Franceschetti, and M Mantegazza. “Self-limited hyperexcitability: Functional effect of a familial hemiplegic migraine mutation of the Nav1.1 (SCN1A) Na<sup>+</sup> channel”. In: *J Neurosci* 28.29 (2008), pp. 7273–7283.
- S30. KR Vanmolkot, E Babini, B de Vries, AH Stam, T Freilinger, GM Terwindt, L Norris, et al. “The novel p.L1649Q mutation in the SCN1A epilepsy gene is associated with familial hemiplegic migraine: genetic and functional studies”. In: *Hum Mutat* 28.5 (2007), pp. 522–522.
- S31. M Estacion, C Han, JS Choi, J Hoeijmakers, G Lauria, J Drenth, MM Gerrits, et al. “Intra- and interfamily phenotypic diversity in pain syndromes associated with a gain-of-function variant of Nav1.7”. In: *Mol Pain* 7 (2011), p. 92.
- S32. M Estacion, S Dib-Hajj, P Benke, RH te Morsche, E Eastman, L Macala, J Drenth, et al. “Nav1.7 gain-of-function mutations as a continuum: A1632E displays physiological changes associated with erythromelalgia and paroxysmal extreme pain disorder mutations and produces symptoms of both disorders”. In: *J Neurosci* 28.43 (2008), pp. 11079–11088.
- S33. C Han, AM Rush, SD Dib-Hajj, S Li, Z Xu, Y Wang, L Tyrrell, et al. “Sporadic onset of erythromelalgia: A gain-of-function mutation in Nav1.7”. In: *Ann Neurol* 59.3 (2006), pp. 553–558.
- S34. S Dib-Hajj, A Rush, T Cummins, F Hisama, S Novella, L Tyrrell, L Marshall, et al. “Gain-of-function mutation in Nav1.7 in familial erythromelalgia induces bursting of sensory neurons”. In: *Brain* 128.8 (2005), pp. 1847–1854.
- S35. E Bocksteins, N Ottshytsch, JP Timmermans, A Labro, and D Snyders. “Functional interactions between residues in the S1, S4, and S5 domains of Kv2.1”. In: *Eur Biophys J* 40.6 (2011), pp. 783–793.
- S36. OH Wittekindt, V Visan, H Tomita, F Imtiaz, JJ Gargus, F Lehmann-Horn, S Grissmer, et al. “An apamin- and scyllatoxin-insensitive isoform of the human SK3 channel”. In: *Mol Pharmacol* 65.3 (2004), pp. 788–801.
- S37. TM Ishii, N Nakashima, and H Ohmori. “Tryptophan-scanning mutagenesis in the S1 domain of mammalian HCN channel reveals residues critical for voltage-gated activation”. In: *J Physiol* 579.2 (2007), pp. 291–301.

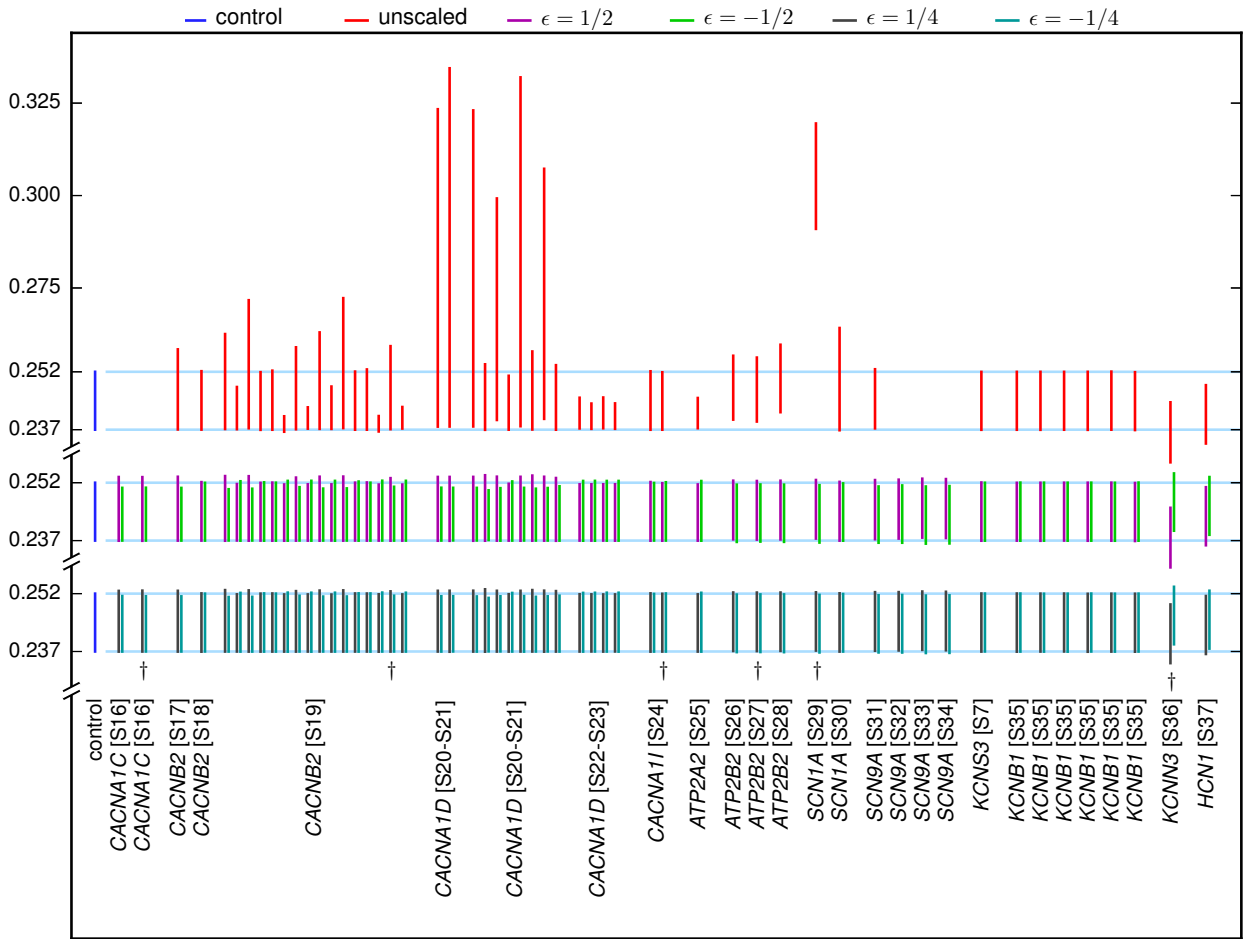


Figure S1: **Ranges of  $\text{Ca}^{2+}$  concentration in simulations of steady-state firing in cells with different genetic variants implemented.** The blue bars (and the light blue horizontal lines) show the minimum and maximum  $\text{Ca}^{2+}$  concentration as a response to a 1.2 nA DC injection in a control neuron, while the other colors show the corresponding quantities in neurons with the variants from Table 2 implemented. The red bars in the upper plot show the effects of the unscaled variants, while the bars in the middle plot show the effects of the  $\epsilon = \frac{1}{2}$  (magenta) and  $\epsilon = -\frac{1}{2}$  (green) downscaled variants. The bars in the lower plot show the effect of minimally scaled (dark gray:  $\epsilon = \frac{1}{4}$ , cyan:  $\epsilon = -\frac{1}{4}$ ) variants. The missing red bars among *CACNA1C* and *SCN9A* variants represent cases where the unscaled variant expresses large depolarization even without an input, and the membrane potential repolarization is missing or too weak to maintain the spiking behavior. The variants are based on previous experimental studies [S7, S16–S37] and they are ordered as in Table 2. The variants marked with † were used in Figures 2–6.

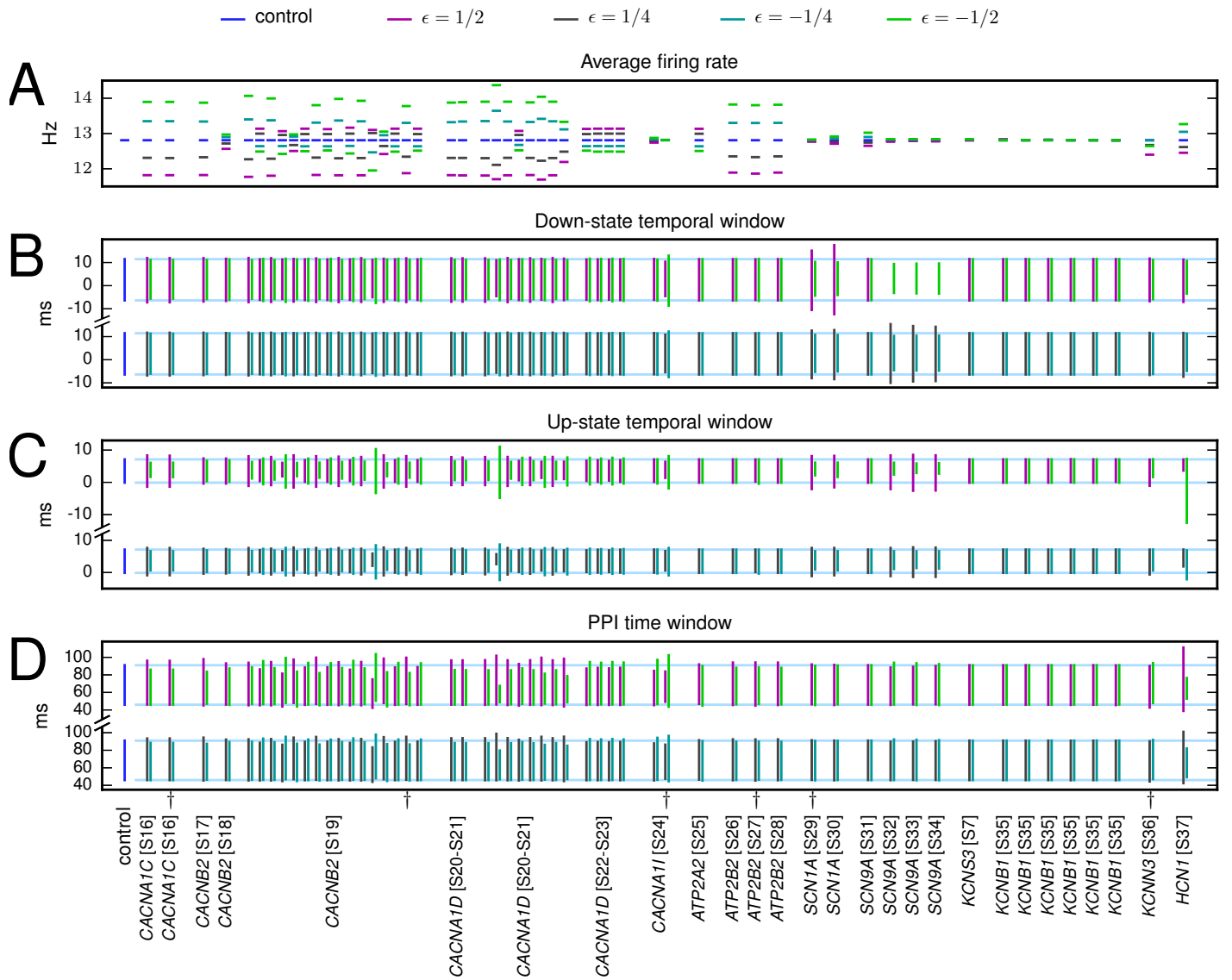
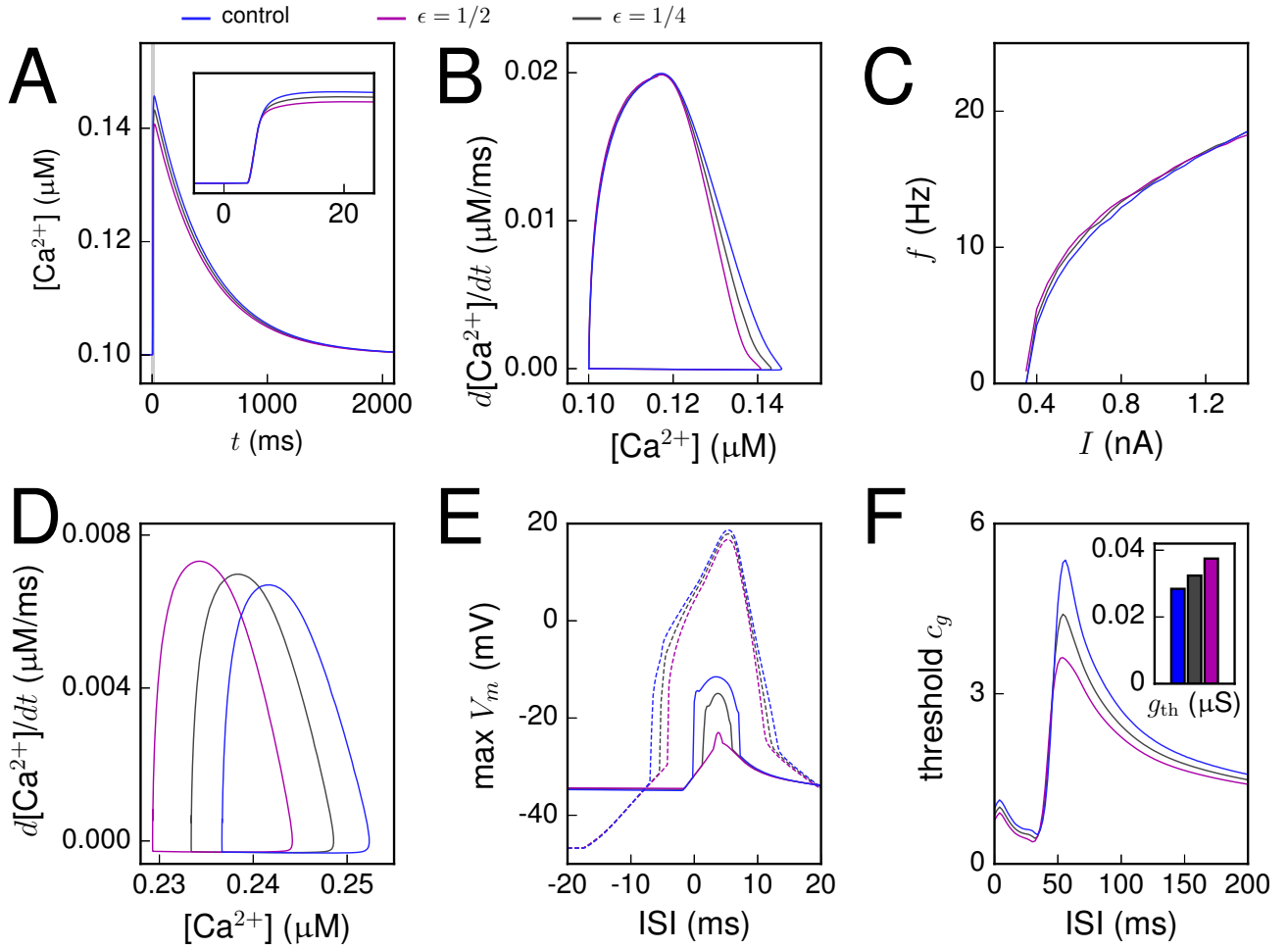


Figure S2: **Various statistics from neurons with different downscaled genetic variants implemented.** **A:** The average steady-state spiking frequency (see Figure 3) when a somatic DC of amplitude 0.35–1.4 nA was injected. Data plotted for each variant in Table 2. **B:** The down-state temporal window span (see Figure 5). The plotted range corresponds to the range of ISIs for which the maximum membrane potential at the apical dendrite was larger than -14.05 mV (the midpoint between the highest and lowest apical dendrite membrane potentials across all ISIs for the control neuron). **C:** The up-state temporal window span (see Figure 5) of ISIs that produced a peak apical dendrite membrane potential larger than -23.21 mV, illustrated in a similar manner as in panel B. **D:** The temporal window for large single-cell prepulse inhibition (PPI, see Figure 6). The plotted ranges correspond to the ISIs for which a larger than three-fold second apical stimulus was required to induce an extra spike. In all panels, the blue bars (and the light blue horizontal lines) correspond to the control neuron values, while the magenta and green bars correspond to the  $\epsilon = \frac{1}{2}$  (magenta) and  $\epsilon = -\frac{1}{2}$  (green) downscaled variants, and the dark gray and cyan bars correspond to the  $\epsilon = \frac{1}{4}$  (dark gray) and  $\epsilon = -\frac{1}{4}$  (cyan) downscaled variants. The missing bars in panel B among *SCN9A* variants correspond to cases where the somatic pulse alone was sufficient to produce a large  $\text{Ca}^{2+}$  spike (apical dendrite membrane potential larger than -14.05 mV). The missing bars in panel C among *CACNB2* and *CACNA1D* variants correspond to cases where no ISI produced a large  $\text{Ca}^{2+}$  spike (i.e., the apical dendrite membrane potential always remained smaller than -23.21 mV). The variants marked with † were used in Figures 2–6.



**Figure S3: Combined genetic variants can radically change the neuron response.** A combination of six downscaled variants from Table 2 (*CACNB2* [S19], *CACNA1D* [S22, S23], *CACNA1I* [S24], *ATP2A2* [S25], and *KCNN3* [S36]) was applied. These variants were chosen as an example combination as they all showed weakened prepulse inhibition (see Figure 6). The gray curves show the properties of a neuron with the combination of  $\epsilon = \frac{1}{4}$  downscaled variants, and the magenta curves represent the combination of  $\epsilon = \frac{1}{2}$  downscaled variants. **A-B:**  $[\text{Ca}^{2+}]$  response to short somatic stimulus, shown in time series (A) and phase plane (B). See Figure 2B and 2C for details. **C:** f-I curves. See Figure 3 for details. **D:**  $[\text{Ca}^{2+}]$  response to prolonged stimulus. See Figure 4 for details. **E:** Integration of apical and somatic stimulus during up and down states. See Figure 5 for details. The combination of  $\epsilon = \frac{1}{2}$  variants did not respond with a strong  $\text{Ca}^{2+}$  spike for any inter-stimulus interval. **F:** Threshold conductance factor for a second spike. See Figure 6 for details. A strong second stimulus with four-fold total conductance with respect to the threshold conductance would always make the neuron with combined  $\epsilon = \frac{1}{2}$  variants spike, while the neuron with combined  $\epsilon = \frac{1}{4}$  variants would inhibit it for  $\text{ISI} \in [49 \text{ ms}, 61 \text{ ms}]$ , and the control neuron would inhibit it for  $\text{ISI} \in [49 \text{ ms}, 71 \text{ ms}]$ .

**Table S2: Effects of positively scaled variants on steady-state firing, integration of somatic and apical inputs, and inhibition of a second apical stimulus.** The shown effects are extracted from the properties of the  $\epsilon = \frac{1}{2}$  variant in Figure S2. The variants are ordered as in Table 2, and the first column shows the name of the underlying gene. The second column shows whether the average firing rate (see Figure S2A) of the variant is increased ('+') or decreased ('-') with respect to the control neuron. A “minuscule” effect refers to cases where the effect was smaller than 0.5% of the control neuron average firing rate. The third and fourth columns show how the down and up-state windows (see Figure S2B–C) are affected in the variant. A “broader” window refers to an effect where the variant window starts at an ISI smaller than the start of the control window and ends at an ISI greater than the end of the control window. By contrast, in a “narrower” case the window starts at an ISI greater than the start of the control window and ends at a smaller ISI than the end of the control window. If both the starting point and end point of the window are moved to the same direction with respect to the control window, the table entry is “moved forward” (toward smaller ISIs) or “delayed” (toward larger ISIs). Cases where both end points moved less than 5% of the width of the temporal window in a control neuron are labeled as “minuscule” effects, regardless the direction to which the end points moved. Finally, the value “N/A” denotes cases where the temporal window could not be defined. The fifth column shows the corresponding properties for the PPI window (see Figure S2D). The variants marked with † are the ones that were used in Figures 2–6. The horizontal lines separate variants that are based on different sets of experimental data, see Table 1.

Gene	f-I curve average	Down-state window	Up-state window	PPI window	
<i>CACNA1C</i>	–	Minuscule	Broader	Delayed	
<i>CACNA1C</i>	–	Minuscule	Broader	Delayed	†
<i>CACNB2</i>	–	Minuscule	Minuscule	Broader	
<i>CACNB2</i>	–	Minuscule	Minuscule	Minuscule	
<i>CACNB2</i>	–	Minuscule	Broader	Broader	
<i>CACNB2</i>	+	Minuscule	Narrower	Moved forward	
<i>CACNB2</i>	–	Minuscule	Broader	Broader	
<i>CACNB2</i>	+	Minuscule	Narrower	Moved forward	
<i>CACNB2</i>	–	Minuscule	Broader	Delayed	
<i>CACNB2</i>	+	Minuscule	Minuscule	Moved forward	
<i>CACNB2</i>	–	Minuscule	Broader	Delayed	
<i>CACNB2</i>	+	Minuscule	Minuscule	Moved forward	
<i>CACNB2</i>	–	Minuscule	Broader	Broader	
<i>CACNB2</i>	+	Minuscule	Narrower	Moved forward	
<i>CACNB2</i>	–	Minuscule	Broader	Broader	
<i>CACNB2</i>	+	Narrower	N/A	Moved forward	
<i>CACNB2</i>	–	Minuscule	Broader	Delayed	
<i>CACNB2</i>	+	Minuscule	Minuscule	Moved forward	
<i>CACNB2</i>	–	Minuscule	Broader	Delayed	†
<i>CACNB2</i>	+	Minuscule	Minuscule	Minuscule	
<i>CACNA1D</i>	–	Minuscule	Broader	Delayed	
<i>CACNA1D</i>	–	Minuscule	Broader	Broader	
<i>CACNA1D</i>	–	Minuscule	Broader	Broader	
<i>CACNA1D</i>	–	Narrower	N/A	Delayed	
<i>CACNA1D</i>	–	Minuscule	Broader	Broader	
<i>CACNA1D</i>	+	Minuscule	Narrower	Minuscule	
<i>CACNA1D</i>	–	Minuscule	Broader	Broader	
<i>CACNA1D</i>	–	Minuscule	Narrower	Broader	
<i>CACNA1D</i>	–	Minuscule	Broader	Broader	
<i>CACNA1D</i>	–	Minuscule	Narrower	Broader	
<i>CACNA1D</i>	+	Minuscule	Narrower	Moved forward	
<i>CACNA1D</i>	+	Minuscule	Minuscule	Moved forward	
<i>CACNA1D</i>	+	Minuscule	Narrower	Moved forward	
<i>CACNA1D</i>	+	Minuscule	Minuscule	Moved forward	
<i>CACNA1I</i>	–	Minuscule	Minuscule	Moved forward	
<i>CACNA1I</i>	Minuscule	Narrower	Narrower	Narrower	†
<i>ATP2A2</i>	+	Minuscule	Minuscule	Minuscule	
<i>ATP2B2</i>	–	Minuscule	Minuscule	Broader	
<i>ATP2B2</i>	–	Minuscule	Minuscule	Broader	†
<i>ATP2B2</i>	–	Minuscule	Minuscule	Broader	
<i>SCN1A</i>	Minuscule	Broader	Broader	Minuscule	†
<i>SCN1A</i>	–	Broader	Broader	Minuscule	
<i>SCN9A</i>	–	Minuscule	Minuscule	Minuscule	
<i>SCN9A</i>	Minuscule	N/A	Broader	Moved forward	
<i>SCN9A</i>	Minuscule	N/A	Broader	Minuscule	
<i>SCN9A</i>	Minuscule	N/A	Broader	Minuscule	
<i>KCNS3</i>	No change	Minuscule	Minuscule	Minuscule	
<i>KCNB1</i>	Minuscule	Minuscule	Minuscule	Minuscule	
<i>KCNB1</i>	No change	Minuscule	Minuscule	Minuscule	
<i>KCNB1</i>	Minuscule	Minuscule	Minuscule	Minuscule	
<i>KCNB1</i>	No change	Minuscule	Minuscule	Minuscule	
<i>KCNB1</i>	No change	Minuscule	Minuscule	Minuscule	
<i>KCNB1</i>	Minuscule	Minuscule	Minuscule	Minuscule	
<i>KCNN3</i>	–	Minuscule	Moved forward	Moved forward	†
<i>HCN1</i>	–	Minuscule	Narrower	Broader	

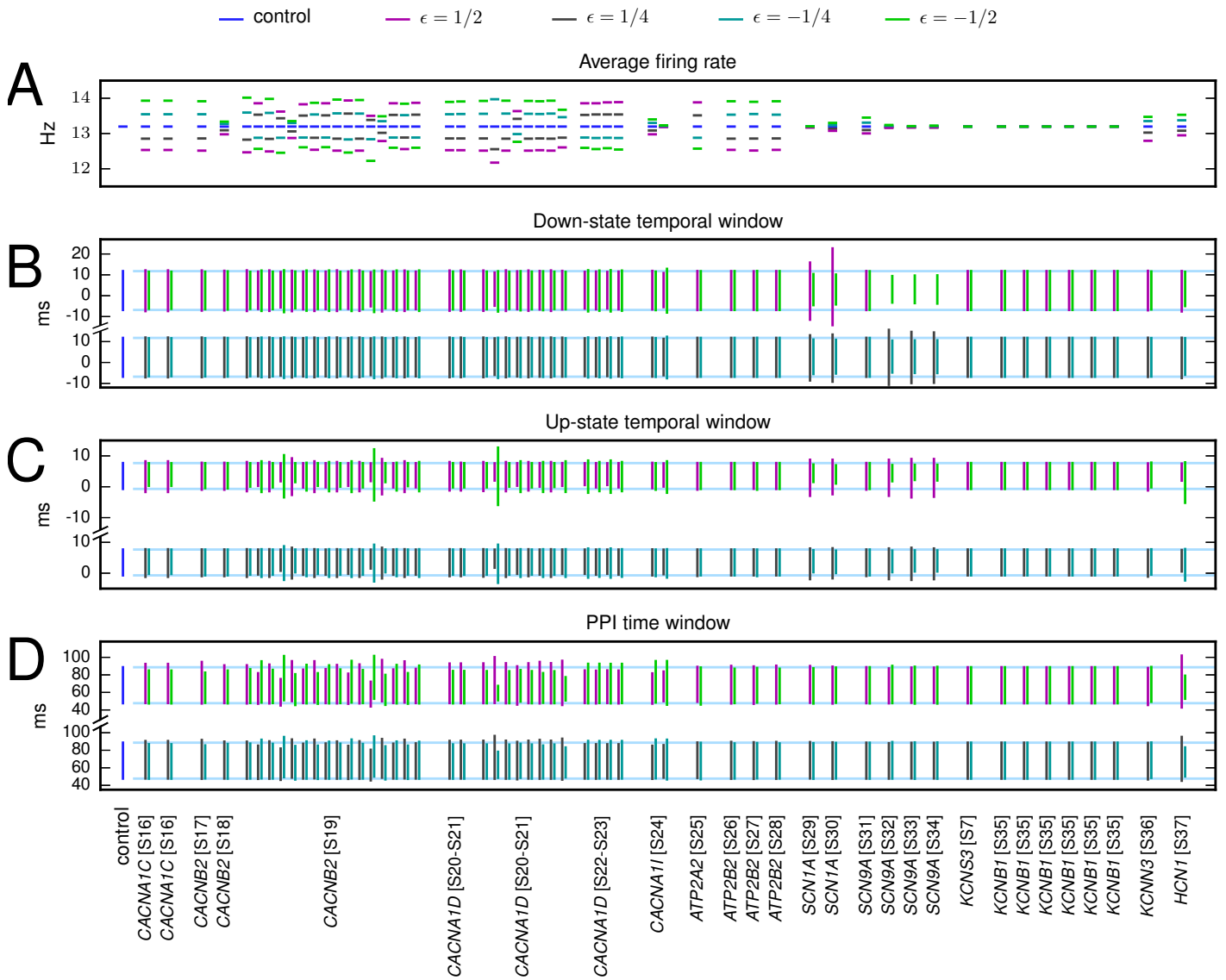


Figure S4: **Various statistics from neurons with alternative set of fitted model parameters and different downscaled genetic variants implemented.** The maximal conductances and parameters controlling  $\text{Ca}^{2+}$  dynamics from Table S1 in [S2] (“Model 1”) were applied, while other parameters were kept fixed. **A:** The average steady-state spiking frequency when a somatic DC of amplitude 0.35–1.4 nA was injected. See Figure S2A for the corresponding results in the neuron model with default parameters. **B:** The down-state temporal window span. See Figure S2B. **C:** The up-state temporal window span. See Figure S2C. **D:** The temporal window for large single-cell prepulse inhibition. See Figure S2D.

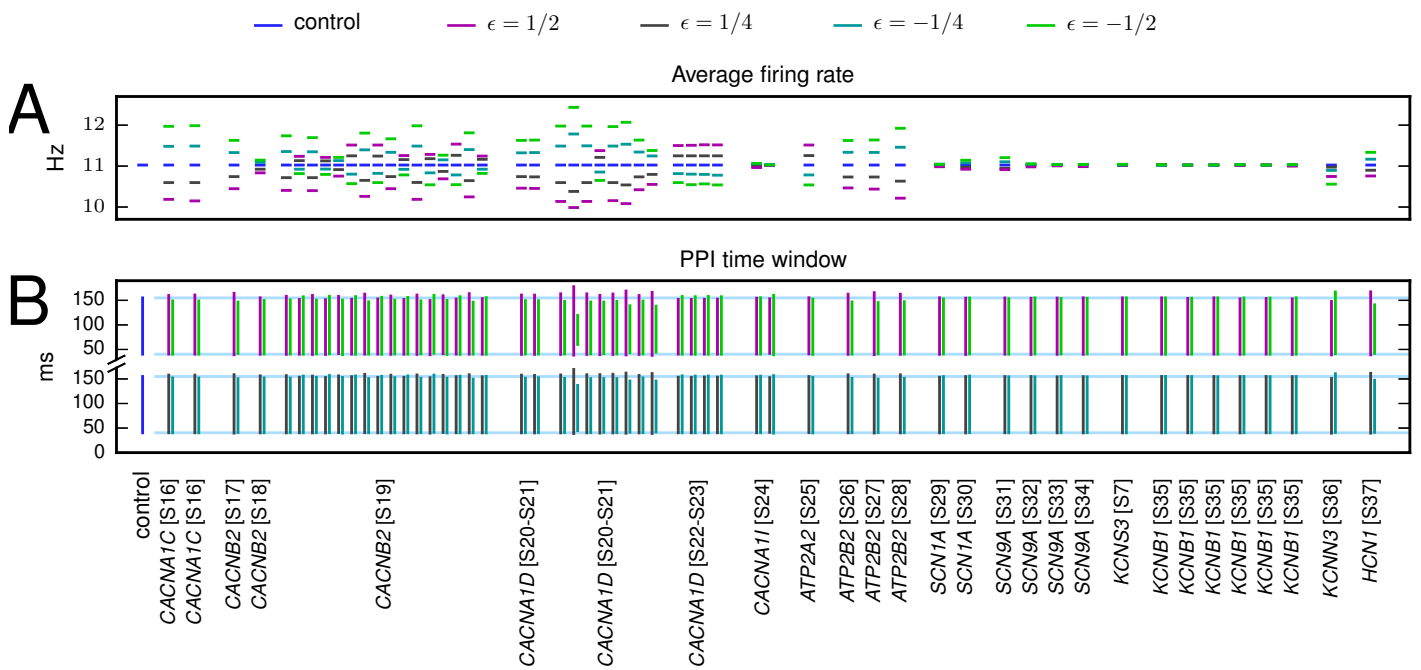


Figure S5: **Average firing frequency and PPI statistics from neurons with alternative morphology and different downscaled genetic variants implemented.** The cell morphology #2 of [S2] was used with the default model parameters. **A:** The average steady-state spiking frequency when a somatic DC of amplitude 0.35–1.4 nA was injected. See Figure S2A for the corresponding results in cell #1. **B:** The temporal window for large single-cell prepulse inhibition. See Figure S2D. The plotted ranges correspond to the ISIs for which a larger than 1.5-fold second apical stimulus was required to induce an extra spike.